Journal of Energy Storage 72 (2023) 108428

Contents lists available at ScienceDirect

Journal of Energy Storage

journal homepage: www.elsevier.com/locate/est

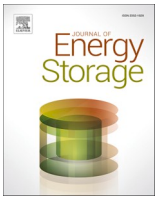

Analysis of the discharging process of latent heat thermal energy storage units by means of normalized power parameters

Andreas König-Haagen [a,c,*], Stephan Höhlein [a], Ana Lázaro [b], Mónica Delgado [b], Gonzalo Diarce [c], Dominic Groulx [d], Florent Herbinger [d], Ajinkya Patil [d], Gerald Englmair [e], Gang Wang [e], Amir Abdi [f], Justin N.W. Chiu [f], Tianhao Xu [f], Christoph Rathgeber [g], Simon Pöllinger [g], Stefan Gschwander [h], Sebastian Gamisch [h]

[a] Chair of Engineering Thermodynamics and Transport Processes (LTTT), Center of Energy Technology (ZET), University of Bayreuth, Bayreuth, Germany
[b] Aragón Institute for Engineering Research (I3A), Thermal Engineering and Energy Systems Group, University of Zaragoza, Zaragoza, Spain
[c] ENEDI Research Group, Department of Energy Engineering, Faculty of Engineering of Bilbao, University of the Basque Country UPV/EHU, Bilbao, Spain
[d] Lab of Applied Multiphase Thermal Engineering (LAMTE), Dalhousie University, 5269 Morris St., B3H 4R2 Halifax, Canada
[e] Department of Civil Engineering, Technical University of Denmark (DTU), Brovej, Building 118, 2800 Kgs. Lyngby, Denmark
[f] Department of Energy Technology, KTH-Royal Institute of Technology, Stockholm, Sweden
[g] Bavarian Center for Applied Energy Research (ZAE Bayern), Walther-Meißner-Str. 6, 85748 Garching, Germany
[h] Fraunhofer Institute for Solar Energy Systems ISE, Heidenhofstr. 2, 79110 Freiburg, Germany

ARTICLE INFO

Keywords:
Power
Evaluation
Performance indicators
Phase change materials
Latent heat
Thermal energy storage

ABSTRACT

Many efforts are being made to mitigate the main disadvantage of most phase change materials – their low thermal conductivities – in order to deliver latent heat energy storage systems (LHESS) with adequate performance. However, the effect of applied methods is difficult to compare as they are mostly tested for different storage types and sizes and/or different boundary and initial conditions, which hinders rapid progress in the optimization of these approaches. In this work, a previously developed method for comparing the performance of LHESS is applied to experimental results of different storage systems under different conditions and subsequently analyzed and further refined. The main idea of the method is to normalize the power with the volume and a reference temperature difference and compare its mean value plotted over the normalized mean capacity flow of the heat transfer fluid (HTF). This enables the presentation of the results in a compact and easily comparative way. Attention has to be paid when it comes to the choice of the reference temperature difference, the reference volume and the method for calculating the mean value. Two variants of calculating the mean value (time-weighted and energy-weighted) and two variants of reference temperatures for determining the temperature difference to the inlet temperature of the HTF (initial temperature and melting temperature) are applied and discussed in detail. While the method significantly increases the comparability of results, none of the options listed above are without drawbacks. Approaches are shown to reduce or eliminate these drawbacks in the future. The recommendation for comparing different LHESS under different conditions is to use the method described here and clearly state the chosen reference temperature, reference volume and method for calculating the mean value.

1. Introduction

Thermal energy storage (TES) systems present important opportunities to increase the efficiency of thermal systems, the integration of renewable energies, the utilization of waste heat, and the temperature control of various systems, including electronics. Those systems using phase change materials (PCMs), defined as Latent Heat Energy Storage Systems (LHESS), offer the additional advantages of an increased energy storage density over the phase change transition temperature of the PCM used and operation over a narrower range of temperatures.

However, PCMs have, for the most part, low thermal conductivities, which leads to inherently low heat transfer rates in and out of an LHESS, also known as the rate problem [1]. Many solutions have been and

* Corresponding author at: Chair of Engineering Thermodynamics and Transport Processes (LTTT), Center of Energy Technology (ZET), University of Bayreuth, Bayreuth, Germany.
E-mail address: andreas_knig001@ehu.eus (A. König-Haagen).

https://doi.org/10.1016/j.est.2023.108428
Received 2 March 2022; Received in revised form 5 September 2022; Accepted 17 July 2023
Available online 2 August 2023

Nomenclature

Variables and abbreviations

$\dot{C}$	Capacity flow in W/K
$\overline{\dot{C}}$	Mean of the capacity flow in $W/(m^3K)$
c_p	Specific heat capacity in $J/(kgK)$
ε	Effectivity
HTF	Heat Transfer Fluid
LHESS	latent heat energy storage systems
$\dot{m}$	Mass flow in kg/s
NTU	Number of transfer units
Q	Heat in J
$\dot{Q}$	Thermal power in W
$\overline{\dot{Q}}$	Mean value of the thermal power in W
$\left\lvert\overline{\dot{Q}}\right\rvert$	Absolute mean value of the thermal power in W
PCM	Phase change material
Ste	Stefan number
t	Time in s
Δt	Time step size in s
T	Temperature in K
TES	Thermal energy storage
UA	Heat transfer coefficient times the area in W/K
V	Volume in m^3

Subscripts

end	End of experiment
energy	Energy-weighted
HEX	heat exchanger
HTF	Heat transfer fluid
initial	Initial condition
inlet	Inlet condition
INS	insulation
melt	Melting
PCM	Phase change material
ref	Reference
time	Time-weighted
TOT	Total volume
start	Start of experiment

superscripts

exp1	Example 1
exp2	Example 2
exp3	Example 3
exp4	Example 4
norm	normalized

continue to be studied for the purpose of increasing the heat transfer rates through the utilization of highly thermally conductive particles [2–4], metal foams and matrices [5–7], graphite matrices [8–10], macro-encapsulation [11,12], and design decisions looking at geometries and the addition of fins [13–17] or alternative structures [14,18]. Overviews of these techniques can be found in several reviews [19–21] and alternative approaches are listed in a recent publication [22].

Numerous individual studies have been done to characterize given LHESS that use different heat exchange systems as a function of the PCM used and varying operating parameters (temperatures, flow rates, etc.), during both the charging and discharging phases [15,23–29].

Looking at the range of data obtained from these studies raises an important problem: how can the performance of different LHESS (different geometries, heat exchange systems, PCMs, operating parameters) be compared? However, it must be remembered that the ability to quantitatively compare different LHESS systems is a prerequisite to developing any design rules for such systems [26].

The characterization of LHESS as a function of operating parameters results in power curves ($\dot{Q}$ vs time) that can be integrated to give energy storage curves (Q vs time). However, such curves are ineffective when comparing systems of different sizes or operating over largely different temperature ranges, i.e., for example, they do not help answer the simple question: is the larger system providing higher total heat transfer rates because of its size, or because it has a better design?

Earlier work looked at comparative metrics and design rules from traditional heat exchangers for inspiration. This led to studies aimed at applying the effectiveness (ε) to LHESS using PCM-heat exchangers [30,31], which were originally conducted for designing LHESS [32]. Issues related to the definition of effectiveness when applied to transient problems where the maximum possible heat transfer rate cannot be defined a priori were raised [26]. Ultimately, the effectiveness was applied over a narrow range of the charging or discharging process, when the bulk of the PCM is at a fairly constant temperature [33]. Using the number of transfer units (NTU), the other half of the traditional ε-NTU method, or UA-values, could also be problematic since the heat transfer coefficient in the PCM can change over time, as conduction gives way to natural convection during melting, or the overall conduction thermal resistance increases during solidification. However, it has been found from previous studies that presenting the results over a dimensionless time [7,34] increases comparability. The same may hold for the melt fraction for small Stefan numbers Ste, however, the melt fraction can be hard to determine in experiments. In addition, Lázaro et al. have presented an averaging approach that could be applied to determine a system specific UA-value [35].

A system's power characteristics still appear to be a natural comparative metric. Again, Lázaro et al. [35] presented an approach based on previous work [36,37] that first looks at the power in or out of the system as a function of the energy stored or discharged, in order to reduce the system to one mean power value ($\overline{\dot{Q}}$), which is obtained by integrating the power as a function of the energy.

Knowing that energetic and economic aspects are also of crucial importance for LHESS and that therefore power considerations alone are, by far, not sufficient for a complete evaluation of such systems, this work is limited to the consideration of power. The study is based on preliminary work conducted by the authors as part of Subtask 4P of the IEA SHC Task 58/Annex 33 [38]. It presents an analysis of the discharging (solidification) of different LHESS based on PCM-heat exchangers, on which the approach defined by Lázaro et al. [35] is applied and analyzed in detail. The mean and normalized power parameters are calculated in different ways, and the results are considered to look at the possibility of using those parameters as comparative metrics. The paper is structured as follows. After the introduction, the method applied is described in Section 2. The study involves more than 30 experimental results from eleven setups, which are introduced in Section 3. In Section 4, the results are presented and discussed and, finally, a conclusion is given in Section 5.

2. Method

2.1. Performance parameters

As described above, *UA* and $\dot{Q}$ might be suitable to define performance parameters that allow for a fair comparison of different LHESS designs over different operating parameters. Within this work the focus is on $\dot{Q}$. The main idea is to normalize $\dot{Q}$ where possible, calculate the mean values and present it in an easily interpretable way. It is assumed

that the power is linearly dependent on the volume V and that the same is true for to the temperature difference. This means that the influence of free convection (as solidification is considered), radiation and temperature-dependent material properties are neglected. Therefore, the normalized power $\dot{Q}^{norm}$ is calculated by

$$\dot{Q}^{norm} = \frac{\dot{Q}}{V \bullet \left(T_{inlet} - T_{ref}\right)} \tag{1}$$

with T_{inlet} and T_{ref} being the inlet temperature of the HTF and a reference temperature of the LHESS, respectively. The choice of T_{ref} is essential. The results presented in this paper are calculated with $T_{ref} = T_{initial}$ and are also given for $T_{ref} = T_{melt}$ in the Supplementary Material S3: Additional Results. A discussion of both choices for T_{ref} can be found in Section 4.1.2. The definition of the volume V is also of great importance. To calculate the results for this paper, the volume was set to $V = V_{PCM} + V_{HTF}$ (and to $V = V_{PCM} + V_{HTF} + V_{HEX}$ for two setups where $V_{PCM} + V_{HTF}$ is not known). A discussion on using other definitions can be found in Section 4.1.4. For calculating a normalized mean value of the power $\overline{\dot{Q}^{norm}}$, two approaches are investigated. Either a calculation performed as time-weighted

$$\overline{\dot{Q}^{norm}_{time}} = \frac{\int_{t_{start}}^{t_{end}} \dot{Q}^{norm}\, dt}{t_{end} - t_{start}} \cong \frac{\sum_{t_{start}}^{t_{end}} \left(\dot{Q}^{norm} \bullet \Delta t\right)}{t_{end} - t_{start}} \tag{2}$$

or as energy-weighted

$$\overline{\dot{Q}^{norm}_{energy}} = \frac{\int_{t_{start}}^{t_{end}} \dot{Q}^{norm} \bullet \dot{Q}^{norm}\, dt}{Q^{norm}} \cong \frac{\sum_{t_{start}}^{t_{end}} \left(\dot{Q}^{norm} \bullet \left(\dot{Q}^{norm} \bullet \Delta t\right)\right)}{\sum_{t_{start}}^{t_{end}} \left(\dot{Q}^{norm} \bullet \Delta t\right)}. \tag{3}$$

The integration limit is set at 95 % of the energy or at the time when 95 % of the energy is discharged. The reference of 100 % is set at the amount of energy discharged at the end of the experiment. In some discharge experiments, an inlet temperature above the starting temperature occurred briefly at the beginning; this period was not taken into account in the integration. The results are presented later on over a normalized capacity flow $\dot{C}^{norm}$, which is defined as

$$\dot{C}^{norm} = \frac{\dot{m} \bullet c_p}{V}, \tag{4}$$

where the mass flow of the HTF is $\dot{m}$ and its specific heat capacity is c_p. The mean of the normalized capacity flow $\overline{\dot{C}^{norm}}$ can also be calculated as time-weighted

$$\overline{\dot{C}^{norm}_{time}} = \frac{\int_{t_{start}}^{t_{end}} \dot{C}^{norm}\, dt}{t_{end} - t_{start}} \cong \frac{\sum_{t_{start}}^{t_{end}} \left(\dot{C}^{norm} \bullet \Delta t\right)}{t_{end} - t_{start}} \tag{5}$$

or energy-weighted

$$\overline{\dot{C}^{norm}_{energy}} = \frac{\int_{t_{start}}^{t_{end}} \dot{C}^{norm}\, dt}{Q^{norm}} \cong \frac{\sum_{t_{start}}^{t_{end}} \left(\dot{C}^{norm} \bullet \left(\dot{Q}^{norm} \bullet \Delta t\right)\right)}{\sum_{t_{start}}^{t_{end}} \left(\dot{Q}^{norm} \bullet \Delta t\right)}. \tag{6}$$

If $\dot{m}$ is constant then $\overline{\dot{C}^{norm}_{energy}} = \overline{\dot{C}^{norm}_{time}}$ and therefore only $\overline{\dot{C}^{norm}_{energy}}$ is used here, which is also integrated up to 95 % of the energy. Flowcharts for the calculation of $\overline{\dot{Q}^{norm}}$ and $\overline{\dot{C}^{norm}}$ can be found in the Supplementary Material S1: Flowcharts in Fig. S1.1 and Fig. S1.2, respectively.

2.2. The $\overline{\dot{C}^{norm}}/\overline{\dot{Q}^{norm}}$-plot

One of the core pieces of the analysis, performed later, is a diagram developed based on preliminary work [35] in which $\overline{\dot{Q}^{norm}}$ is plotted over $\overline{\dot{C}^{norm}}$. This is done as a normalization in terms of $\dot{m}$, or more generally, $\dot{C}$ cannot be performed in a meaningful way so far, because $\dot{Q}$ is not linearly dependent on $\dot{C}$. Therefore, a normalization is done only for the temperature difference and the volume. The influence of the capacity flow is then shown in a diagram – the $\overline{\dot{C}^{norm}}/\overline{\dot{Q}^{norm}}$-plot. For a better orientation, the analyses and comparison of several types of isolines can be drawn in this diagram. In Fig. 1, lines with a constant $\overline{UA^{norm}}$ are plotted, which indicate the behavior of TES with a constant UA value. For the calculation of these lines, a $\overline{UA^{norm}}$ was first selected and the $\overline{\dot{Q}^{norm}}$ was then calculated for given $\overline{\dot{C}^{norm}}$ values. To do so, the NTU was calculated with

$$NTU = \frac{\overline{UA^{norm}}}{\overline{\dot{C}^{norm}}} \tag{7}$$

and finally, the effectivity ε and $\overline{\dot{Q}^{norm}}$ were subsequently calculated with

$$\varepsilon = 1 - e^{-NTU} = \frac{\overline{\dot{Q}^{norm}}}{\overline{\dot{C}^{norm}}}. \tag{8}$$

Fig. S1.3 in the Supplementary Material S1: Flowcharts consists of a flowchart listing how to plot $\overline{UA^{norm}}$ lines. The diagonal line with an infinite $\overline{UA^{norm}}$ value refers to a direct storage without losses (for instance a perfect hot water puffer storage tank without heat losses and mixing) and defines the benchmark. In this optimal case, $\overline{\dot{Q}^{norm}} = \overline{\dot{C}^{norm}}$ and, from Eq. (7) and Eq. (8), it follows that $\varepsilon = 1$ and $NTU = \infty$, respectively. Most LHESS are a combination of a direct TES (the HTF that is already in the storage) and a part with a finite UA value (the PCM etc). Here, it must be taken into account that the UA value of the PCM etc. is most likely not independent of $\dot{C}$. This is so because, for small $\dot{C}$, the whole length of the LHESS cannot actively participate in the heat transfer process at the same time. Rather, an active part migrates in the flow direction of the HTF through the TES, where its length depends on $\dot{C}$. For these two reasons, it is expected that the behavior of an LHESS does not exactly follow a $\overline{UA^{norm}}$ (iso-line)

3. Experimental setups

In this work, 32 experiments from 11 different setups are presented and analyzed with the approach developed; thereby covering a wide variety of designs as well as sizes – the volume varies over more than two orders of magnitude. The different designs are listed in Table 1 (a more detailed classification can be found in the final report of the IEA SHC Task 58/Annex 33 [38]), while, in Table A.1 in the Appendix A, the initial and boundary conditions of each experiment are shown, as well as general information on the LHESS, the PCM and the HTF, together with the volume of the PCM V_{PCM}, the HTF V_{HTF}, the heat exchanger V_{HEX}, the insulation V_{INS} and the complete LHESS V_{TOT}.

As can be seen in Table 1, designs 3 and 5 include supercooled PCM. A unique aspect for Setup 6 and Setup 7 is that stable supercooling is applied [39]. When using stable supercooling in LHESS, discharging of the stored sensible capacity is typically followed by the discharge of heat of fusion (during PCM solidification) [40]. This storage principle was, for instance, demonstrated in a solar heating system [41,42] and typically results in long periods between charge and discharge cycles – increasing the complexity from the perspective of a comparison with other concepts. Finally, a brief description of each of the eleven setups follows.

3.1. Setup 1

This LHESS consists of a cuboid container in which a total of 72

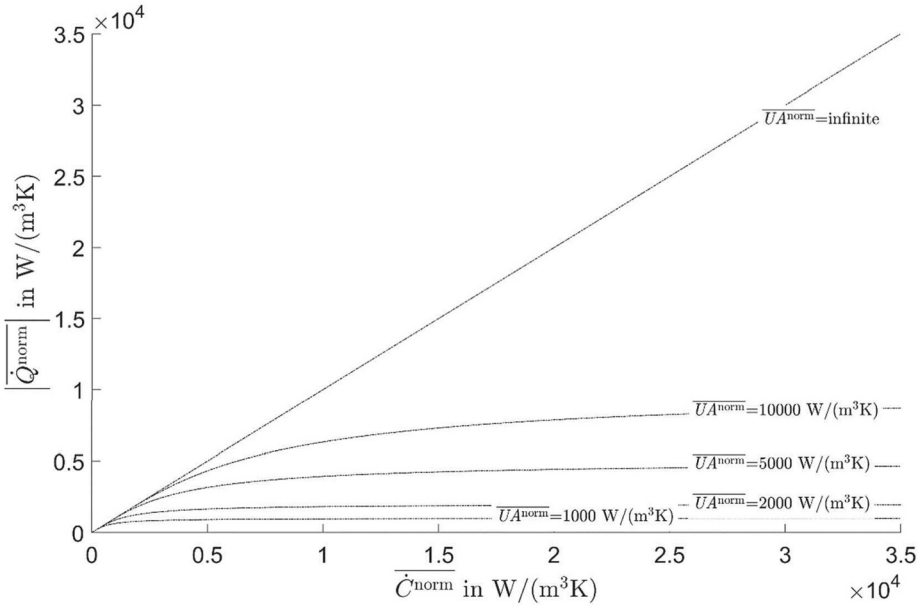

Fig. 1. $\overline{\dot{C}^{\text{norm}}}/\overline{\dot{Q}^{\text{norm}}}$-plot with $\overline{\text{UA}^{\text{norm}}}$ (lines).

Table 1
List of different designs and their identifier.

Identifier	Description
Design 1	Macro encapsulated LHESS with liquid HTF (also tank-in-tank)
Design 2	Macro encapsulated LHESS with gaseous HTF
Design 3	Macro encapsulated LHESS with liquid HTF and supercooled PCM
Design 4	Internal heat exchanger with liquid HTF
Design 5	Internal heat exchanger with liquid HTF and supercooled PCM
Design 6	External heat exchanger with liquid HTF

aluminum capsules, filled with magnesium chloride hexahydrate as PCM, are placed. The capsules are arranged in two levels above each other and have a length of 250 mm and a diameter of 40 mm. The flow direction of the HTF is from bottom to top or vice versa. More information about the LHESS, detailed figures and a description of the experimental procedures can be found in the literature [37].

3.2. Setup 2

This LHTES unit is a PCM-air heat exchanger that consists of a commercially available organic PCM macro-encapsulated in aluminum rigid slabs (CSM panels from Rubitherm filled with RT27 [Rubitherm GmbH. Website, http://www.rubitherm.com/ (under the topic:

Products, Paraffins-RT) [accessed 26.10.10]]). The total amount of PCM in TES is approximately 135 kg, contained in 216 slabs. The slabs are arranged in vertical walls of slabs. These walls are separated from each other by a 1 cm air gap. The air flows in parallel to the slabs containing the PCM. More, detailed information on the experimental results can be found in the literature [28].

3.3. Setup 3

A total of 14 aluminum plates filled with RT60 from Rubitherm are mounted in this LHESS. The plates have the dimensions 22 × 120 × 600 mm^3 and are arranged parallel to each other facing the largest side. Water is used as HTF, which flows in the gaps between the plates. Larrinaga et al. [27] gives more information on this LHESS and the testing procedure.

3.4. Setup 4

A small storage prototype using 1, 2, or 3 copper coils (3/8″ outer diameter) positioned in a rectangular fiberglass box with dimensions 38.75 × 33.7 × 17.75 cm^3 as presented in [43]. Dodecanoic acid (melting temperature of 43 °C) is used as the PCM and water as the HTF. The system was tested over a wide range of initial and HTF temperatures to help determine the impact of each on the storage and discharge performance of the LHESS.

3.5. Setup 5

A small storage prototype using 4, 8 or 12 finned-tubes oriented vertically inside a rectangular fiberglass box with dimensions 30 × 30 × 15.25 cm^3 as presented in [23,44]. Dodecanoic acid (melting temperature of 43 °C) is used as the PCM and water as the HTF. The system was tested over a wide range of initial and HTF temperatures to help determine the impact of each on the storage and discharge performance of the LHESS.

3.6. Setup 6

This storage prototype was tested for combined short and long-term heat storage utilizing stable supercooling [45]. Heat transfer was analyzed in a numerical study [46]. The storage consisted of a cylindrical water vessel of 0.4 m in diameter (without insulation). Inside, 112 tubes with a diameter of 0.0276 m and a length of 1.52 m – containing the composite – were mounted vertically. HTF flows from the bottom to the top of the water vessel. Fig. S2.1 in the Supplementary Material S2: Setups shows the storage prototype without insulation.

3.7. Setup 7

This storage prototype was also tested for utilizing a stable supercooling of sodium acetate trihydrate composite for combined short and long-term heat storage [47]. It was manufactured with inexpensive standard components of water stores. A steel tank with an outer diameter of 0.45 m contained the composite and a steel spiral heat exchanger. It was situated in the center of another steel tank with a diameter of 0.5 m containing HTF – to realize the heat exchange via its outer surface. Fig. S2.2 in the Supplementary Material S2: Setups shows the resulting

"tank-in-tank" design.

3.8. Setup 8

This setup was prepared to visualize the process phase change, including solidification and melting, of a pure organic PCM in a rectangular enclosure enhanced with fins and to measure the rate of heat transfer. Lab grade n-eicosane and tap water were used as the PCM and heat transfer fluid. Fig. S2.3 and Fig. S2.4 in the Supplementary Material S2: Setups show the schematic layout of the set-up and the enclosure.

3.9. Setup 9

The two encapsulated storage setups are in the form of a cylindrical storage vessel with a height of 1350 mm and a diameter of 600 m; the total loaded number of PCM capsules is 160 with the slab encapsulation (Setup 9a, Fig. S2.5 in the Supplementary Material S2: Setups) and 285 with the ellipsoid encapsulation (Setup 9c, Fig. S2.6 in the Supplementary Material S2: Setups). The encapsulated PCM is a commercial product named ATP60, and silica sand is blended as the additive with PCM presumably for increasing the overall thermal conductivity of the filler.

In Setup 9b, a spiral coil was installed into a stainless tank with the dimensions of 720 mm in diameter and 1375 mm in height (see Fig. S2.7 in the Supplementary Material S2: Setups). The heat exchanger used in the spiral coil tank consists of 36 layers of vertically distributed spiral coils. HTF flows through the coils from the inner section and leaves from the outer section.

3.10. Setup 10

A rectangular storage container is used. The heat exchanger is immersed in the PCM and consists of 10 radiator panels arranged in parallel (see Fig. S2.8 in the Supplementary Material S2: Setups). The panels measure $0.3 \times 0.4\ m^2$, with a maximum thickness of 14 mm. The distance between the panels is 16 mm.

3.11. Setup 11

The latent heat storage has a rectangular tank with an internal volume of 1 m^3. A capillary heat exchanger immersed in the PCM, with water as heat transfer medium, is used. Due to the corrosiveness of many salt hydrates, the capillaries are made of polypropylene. To increase both (dis)charging power and storage capacity, the heat exchanger features small distances between the thin capillaries and an overall high surface-to-volume ratio. Fig. S2.9 in the Supplementary Material S2: Setups shows the storage tank with heat exchanger.

4. Results and discussion

The results are presented in two parts. Conceptual aspects are first presented, addressing the question of how the performance parameters should be calculated and presented. In this section, the influence of the initial and boundary condition with respect to temperature will also be discussed, as it is directly connected to the discussion on the choice of T_{ref}. In the second part, the influence of different designs or variations of design aspects and the influence of $\overline{\dot{C}}^{norm}$ is presented.

4.1. Conceptual results

4.1.1. Different ways to plot the power

The simplest way to present the performance of different experiments of various LHESS is to plot $\dot{Q}$ over time, which is shown for all the experiments of this study in Fig. 2. This, however, will in most cases lead to an unfair comparison because of different storage sizes and/or boundary and initial conditions. If a wide variation in $\dot{Q}$ and discharging times exists, as shown for the experiments involved in this study in Fig. 2, it is not even possible to make a meaningful comparison at all.

To allow for a comparison of the performance of the LHESS, $\dot{Q}$ is normalized with Eq. (1) and plotted over relative time and relative energy in Fig. 3. To keep the number of results limited, only one experiment is shown for every setup. The results follow, to a certain extent, the basic presentation of the power curves for different types of LHESS presented in Chapter 5 of Mehling and Cabeza [48]. Using the relative

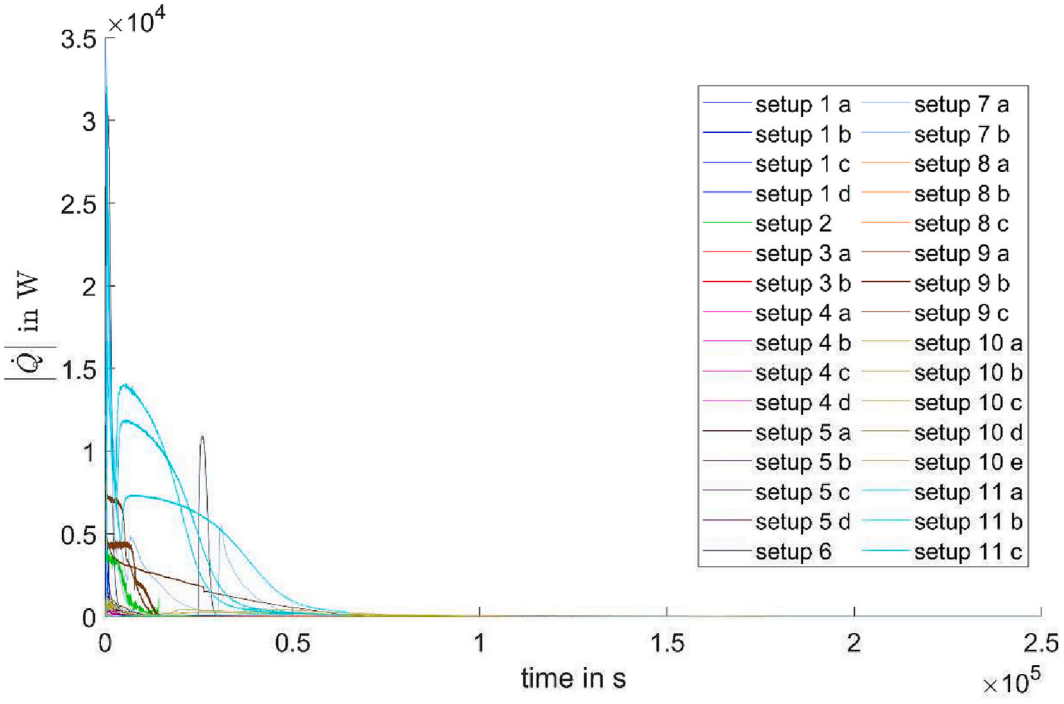

Fig. 2. $\dot{Q}$ over time plotted for all 32 experiments.

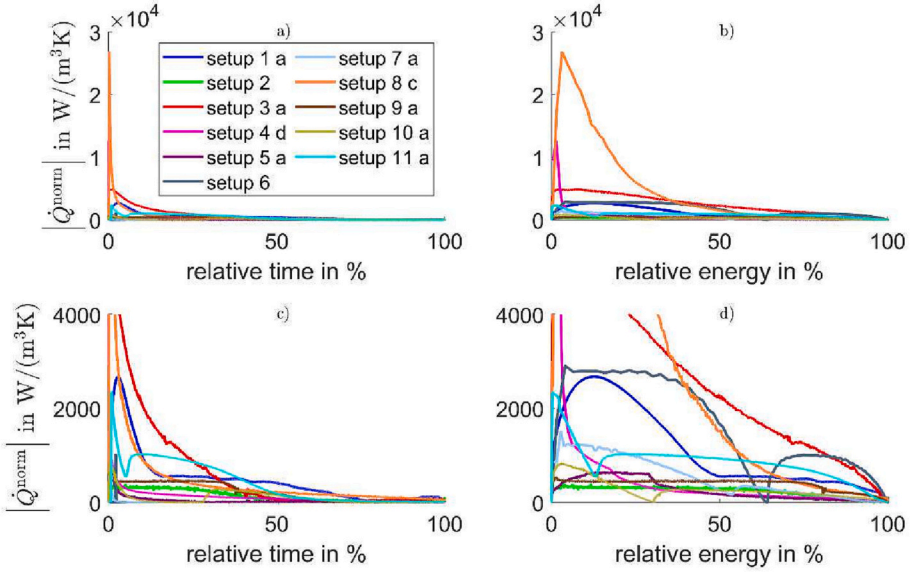

Fig. 3. $\dot{Q}^{norm}$ with $T_{ref} = T_{initial}$ plotted over relative time or over relative energy for one experiment of every setup. The plots c) and d) are zoomed in versions of the plots a) and b) respectively.

energy as the *x*-axis, in particular, allows for a straightforward interpretation of many interesting aspects. Some of these are discussed in detail in the Appendix B.

Plotting the results as in Fig. 3 gives interesting insights, but it has two major drawbacks:

1. The influence of $\dot{m}$ or, more generally speaking, of $\dot{C}$ is neglected.
2. Still, only a rather low number of experiments can be compared.

The approach followed in this paper to overcome these issues is to calculate a mean value of $\dot{Q}^{norm}$ with Eq. (2) (time-weighted) or Eq. (3) (energy-weighted) and to plot it over a mean value of $\dot{C}^{norm}$. The $\overline{\dot{Q}^{norm}_{energy}}$ values of one experiment per setup are shown in Fig. 4.

Now, a larger number of experiments can be compared and the influence of $\overline{\dot{C}^{norm}}$ can be estimated. However, one fundamental question still remains: Is the comparison made in Fig. 3, and especially Fig. 4, fair? First, it should be highlighted again that a comparison in terms of only the power neglects the very important part of the storage density and, of course, the costs of the system, which both need to be taken into account in a holistic analysis. Second, there are several points to investigate and discuss for $\dot{Q}^{norm}$ and $\overline{\dot{Q}^{norm}}$:

1. What is the influence of different T_{ref}?
2. How does the method for calculating the mean value of $\dot{Q}^{norm}$ affect the results?

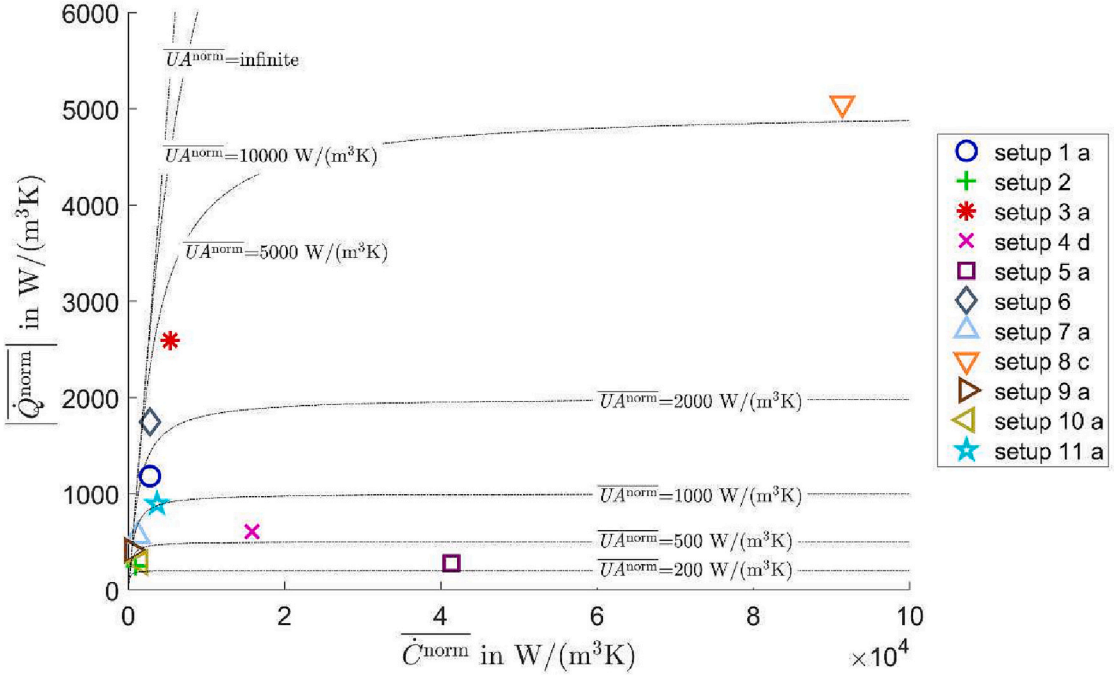

Fig. 4. $\overline{\dot{Q}^{norm}_{energy}}$ with $T_{ref} = T_{initial}$ plotted over $\overline{\dot{C}^{norm}_{energy}}$ for one experiment of every setup.

3. When calculating $\overline{\dot{Q}^{norm}}$ the information on the slope of $\dot{Q}^{norm}$ is lost.
4. What is the influence of different V_{ref}?

All four points are addressed below; the first point in Section 4.1.2, the second and third points in Section 4.1.3, and the last in Section 4.1.4.

4.1.2. Influence of T_{ref}

For normalization in terms of the temperature difference (see Eq. (1)), T_{ref} needs to be defined. Within this work two options, $T_{initial}$ and T_{melt}, are considered for T_{ref}, which are rather easy to determine and constant over time. Furthermore, it is expected that the heat transfer with respect to latent heat corresponds to T_{melt} and that the heat transfer with respect to sensible heat corresponds to $T_{initial}$. A detailed theoretical consideration of the impact of different definitions of T_{ref} is provided in the Appendix C.

Fig. 5 and Fig. 6 show $\overline{\dot{Q}^{norm}_{energy}}$ plotted over $\overline{\dot{C}^{norm}_{energy}}$ for all experiments listed in Table C.1 in the Appendix C for $T_{ref} = T_{initial}$ and $T_{ref} = T_{melt}$, respectively. It can be seen that, generally, the greater the difference between $(T_{initial} - T_{inlet})/(T_{melt} - T_{inlet})$ for the two experiments compared, the more pronounced the contrast between the two choices of T_{ref} will be. For instance, the ratio of $\overline{\dot{Q}^{norm}_{energy}}$ changes most for different T_{ref} for Setup 3 and is almost invisible for Setup 10, which refer to the largest and smallest changes in $\frac{(T_{initial}-T_{inlet})}{(T_{melt}-T_{inlet})}$, respectively.

Here, it should be highlighted that the closer $\overline{\dot{Q}^{norm}_{energy}}$ is for two experiments (that have a variation in the initial and boundary conditions of temperature only), the better the normalization worked. Taking this into account, the normalization with T_{melt} as T_{ref} works better for Setup 1 and Setup 5, while with $T_{initial}$ as T_{ref}, it works better for Setup 3 and Setup 4. For Setup 10, it works well in both cases. It should also be noted that using T_{melt} as T_{ref} leads to unrealistically high UA values for the sensible part of the thermal energy stored. This may result in $\overline{\dot{Q}^{norm}_{energy}}$ being larger than $\overline{\dot{C}^{norm}_{energy}}$, as shown in Fig. 6.

The same results as discussed above are shown for $\overline{\dot{Q}^{norm}_{time}}$ in the Supplementary Material S3: Additional Results in Fig. S3.1 and Fig. S3.2 for $T_{ref} = T_{initial}$ and $T_{ref} = T_{melt}$, respectively. In this case, regardless of the choice of T_{ref}, the normalization performs well for Setup 4, Setup 5 and Setup 10, but does not work for Setup 1 or Setup 3.

Next, $\dot{Q}^{norm}$ is plotted over the relative energy, once with $T_{ref} = T_{initial}$ (see Fig. 7) and once with $T_{ref} = T_{melt}$ (see Fig. 8). The experiments of Setup 1, Setup 3 and Setup 4 have a distinctive peak of $\dot{Q}^{norm}$ in the beginning, which refers to the sensible heat of the HTF and potentially the encapsulation as well. Comparing this peak for different experiments of one setup shows that, with $T_{ref} = T_{initial}$ (see Fig. 7), the normalization works for this part of the discharging process. Setting $T_{ref} = T_{melt}$ (see Fig. 8), the normalization in the sensible part does not perform well, but for the part of the discharging process where latent heat plays a major role – i.e., after the initial peak – it generally gives better results than setting $T_{ref} = T_{initial}$.

The main advantages and disadvantages of using $T_{initial}$ or T_{melt} as the reference temperature are listed in Table 2. Neither choice is perfect, but both produce results that are more comparable than without normalization. In general, a normalization of several experiments is more comparable when the experiments involved show a proportional temperature change (see Appendix C for definition) between each other and similar Ste. In any case, the type of reference temperature used needs to be clearly identified and should be identical for the experiments involved, and the above described effects of the two reference temperatures should be taken into account when applying a normalization.

Finally, it should be noted that the normalization for $\overline{\dot{Q}^{norm}}$ might be improved by calculating T_{ref} through weighting $T_{initial}$ and T_{melt} with respect to the ratio of latent to sensible heat. However, comprehensive tests need to be done to check this assumption. Moreover, no matter the choice of T_{ref}, there will be an error in the normalization when plotting

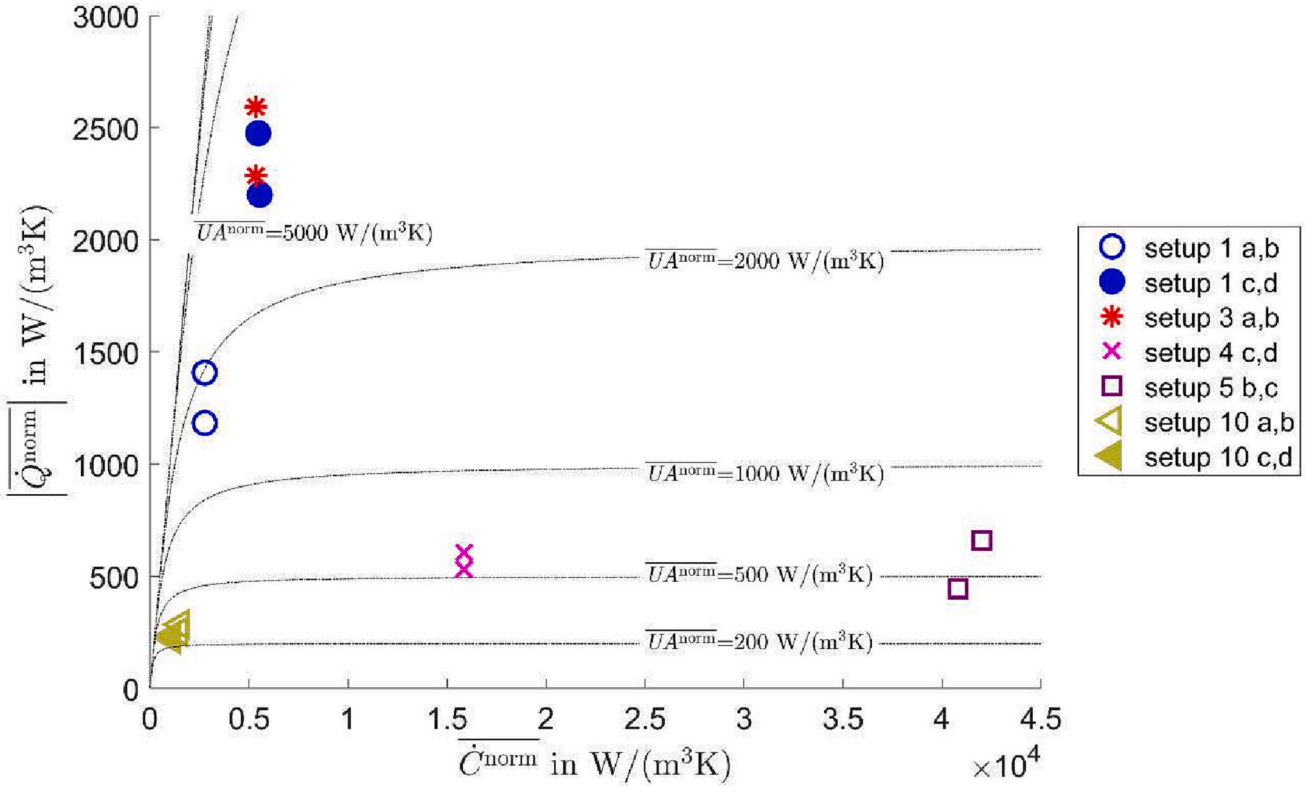

Fig. 5. $\overline{\dot{Q}^{norm}_{energy}}$ with $T_{ref} = T_{initial}$ plotted over $\overline{\dot{C}^{norm}_{energy}}$ for experiments with different boundary and initial conditions of temperature.

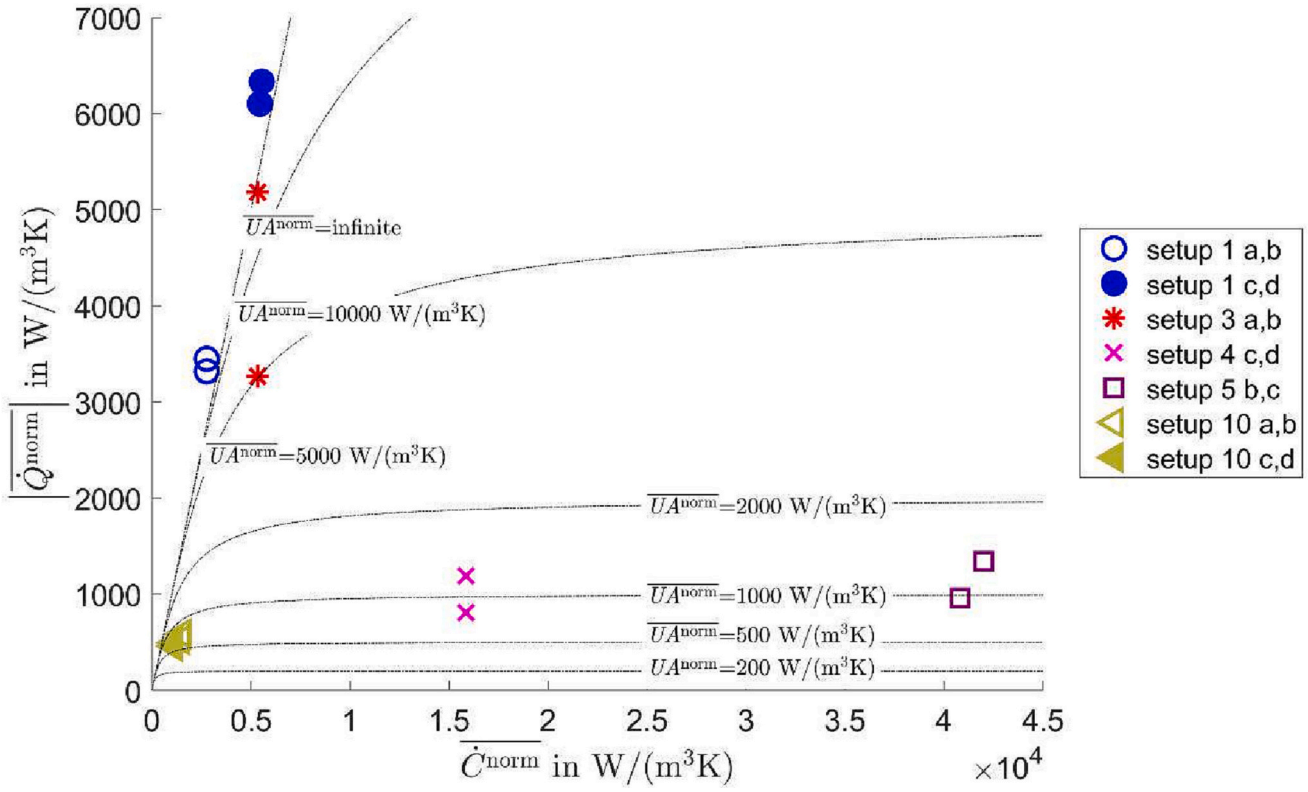

Fig. 6. $\overline{\dot{Q}^{\mathrm{norm}}_{\mathrm{energy}}}$ with $T_{\mathrm{ref}} = T_{\mathrm{melt}}$ plotted over $\overline{\dot{C}^{\mathrm{norm}}_{\mathrm{energy}}}$ for experiments with different boundary and initial conditions of temperature.

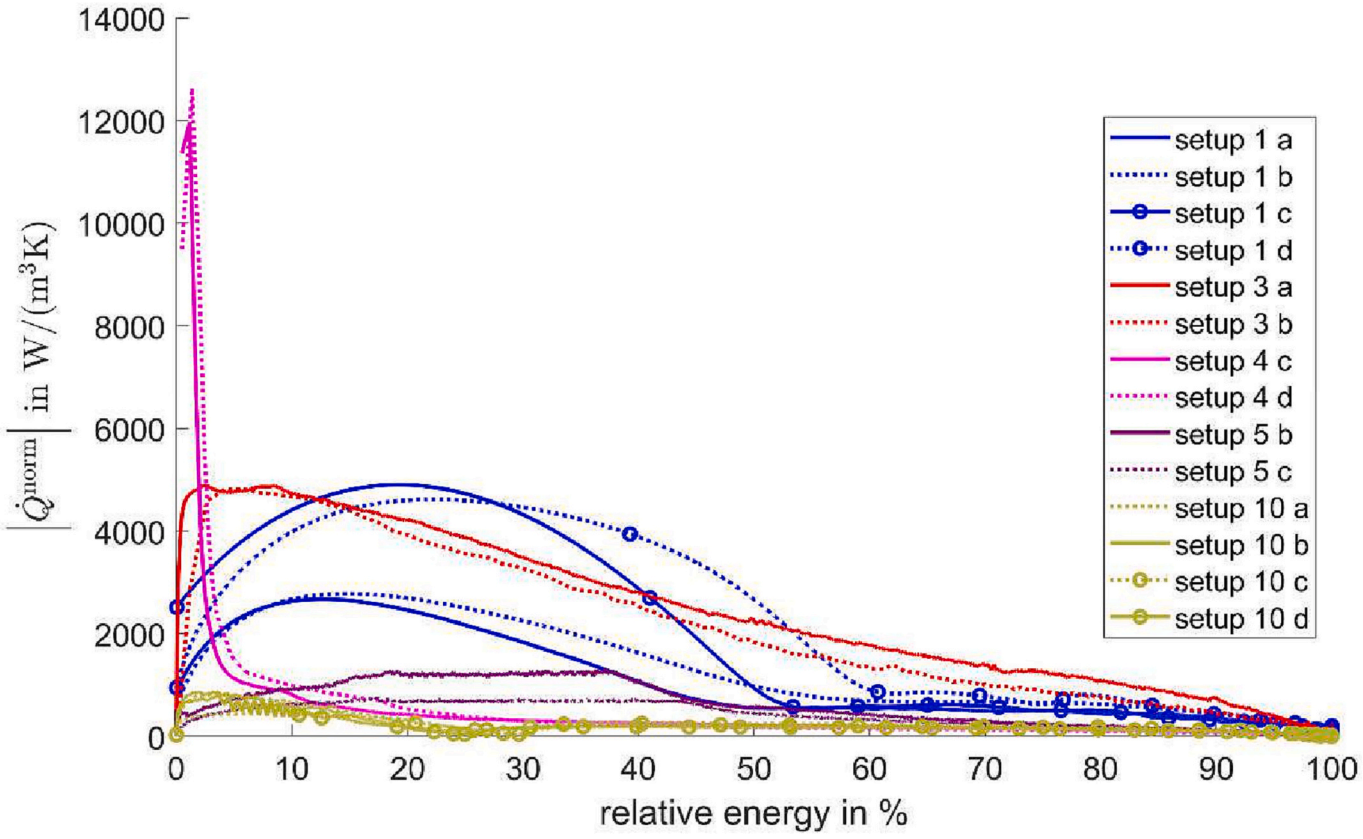

Fig. 7. $\dot{Q}^{\mathrm{norm}}$ with $T_{\mathrm{ref}} = T_{\mathrm{initial}}$ plotted over relative energy for experiments with different boundary and initial conditions of temperature.

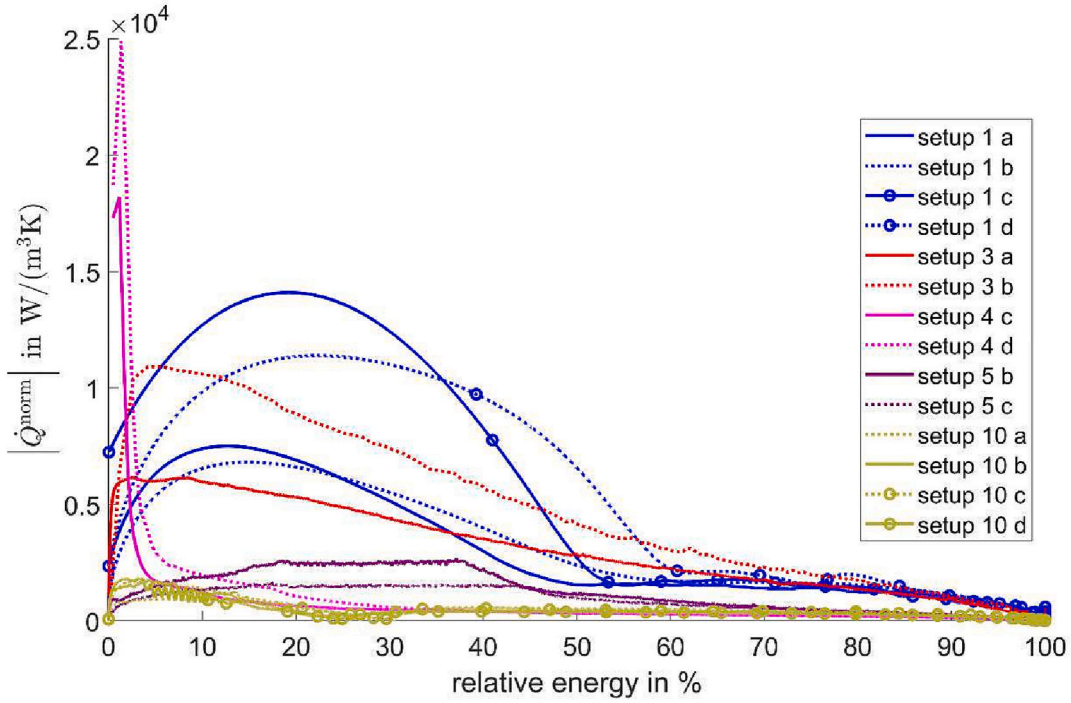

Fig. 8. $\dot{Q}^{norm}$ with $T_{ref} = T_{melt}$ plotted over relative energy for experiments with different boundary and initial conditions of temperature.

Table 2
Advantages and disadvantages of using $T_{initial}$ or T_{melt} as reference temperature.

$T_{inlet} - T_{initial}$	$T_{inlet} - T_{melt}$
+ Reflects the boundary conditions of the application	+ Reflects the heat transfer concerning the latent heat of the PCM ➔ works especially well for small Ste
+ Is independent of the storage type and storage material	+ Is a fixed temperature and easy to define (for pure PCM that do not supercool)
+ Reflects the discharging of the HTF and results in an effectivity of 1 for an ideal direct storage	
- The initial temperature might be hard to measure	- Comparison with STES or LHESS with multiple PCM is difficult
- Does not reflect the heat transfer with the PCM concerning the latent heat. If the temperatures are symmetrical, the temperature difference applied is twice as high as the temperature difference $T_{inlet} - T_{melt}$.	- Does not reflect the power of the HTF initially in the LHESS. If the temperatures are symmetrical, the temperature difference applied is half the temperature difference $T_{inlet} - T_{initial}$.
- Leads to "unfair" results as soon as $\frac{T_{inlet} - T_{melt}}{T_{inlet} - T_{initial}}$ is not equal for the compared experiments. Also, differing Ste can give problems.	- Leads to "unfair" results as soon as $\frac{T_{inlet} - T_{melt}}{T_{inlet} - T_{initial}}$ is not equal for the compared experiments. Also, differing Ste can give problems.
	- Can lead to an effectivity greater than 1 and ill-defined logarithmic temperature differences within the calculation of the UA values

the slope of $\dot{Q}^{norm}$, for instance over relative energy, as the ratio of sensible to latent heat changes during the charging or discharging process.

4.1.3. Influence of the mean value calculation

Two ways to calculate the mean value of $\dot{Q}^{norm}$ are investigated in this study – a time-weighted and an energy-weighted $\overline{\dot{Q}^{norm}}$. A theoretical discussion on both choices can be found in Appendix D.

The advantages and disadvantages of both approaches for calculating the mean of $\dot{Q}^{norm}$ are listed in Table 3. Which advantages and disadvantages outweigh the others cannot be clearly determined at this point. Therefore, throughout this paper, the results are presented with $\overline{\dot{Q}^{norm}_{energy}}$ and additionally with $\overline{\dot{Q}^{norm}_{time}}$ in the Supplementary Material S3: Additional Results. Furthermore, for future work, it is recommended to always clearly indicate the selected method when making a comparison.

As already mentioned, by doing a mean value calculation of $\dot{Q}^{norm}$, the information on its slope is lost. One option to overcome this drawback might be to plot and compare $\overline{\dot{Q}^{norm}_{energy}}$ as well as $\overline{\dot{Q}^{norm}_{time}}$ (see Fig. 9 and, for $T_{ref} = T_{melt}$, Fig. S3.3 in the Supplementary Material S3: Additional Results). When comparing the results presented in Fig. 9 with the $\dot{Q}^{norm}$ plots over relative energy (see Fig. 3 b and d) it seems that $\overline{\dot{Q}^{norm}_{energy}}/\overline{\dot{Q}^{norm}_{time}}$ works as an indicator for specifying if $\dot{Q}^{norm}$ is rather constant during the discharging process or whether it changes a lot. Qualitatively speaking, the closer $\overline{\dot{Q}^{norm}_{energy}}/\overline{\dot{Q}^{norm}_{time}}$ is to 1, the more constant $\dot{Q}^{norm}$ is. For instance, the experiments Setup 4d, Setup 3a, Setup 1a and Setup 6 give $\overline{\dot{Q}^{norm}_{energy}}/\overline{\dot{Q}^{norm}_{time}}$ values distinctively larger than 1 (see Fig. 9) and all of them exhibit a large change in $\dot{Q}^{norm}$ (see Fig. 3 b and d). Compared to these,

Table 3
Advantages and disadvantages of using energy or time-weighted $\overline{\dot{Q}^{norm.}}$

Energy-weighted averaging	Time-weighted averaging
+ Is less sensitive to the stopping criteria	+ Reflects the actual mean power, which would be used for designing LHESS.
- The deduced $\overline{\dot{Q}^{norm}_{energy}}$ over-predicts the mean power over time, which is used to design LHESS.	- The deduced $\overline{\dot{Q}^{norm}_{time}}$ may strongly depend on the stopping criteria and approaches 0 for complete discharging.
- LHESS with an initial high power and later a low power tend to perform better than LHESS with constant power.	- All information on the slope of the power curve is lost
- All information on the slope of the power curve is lost	

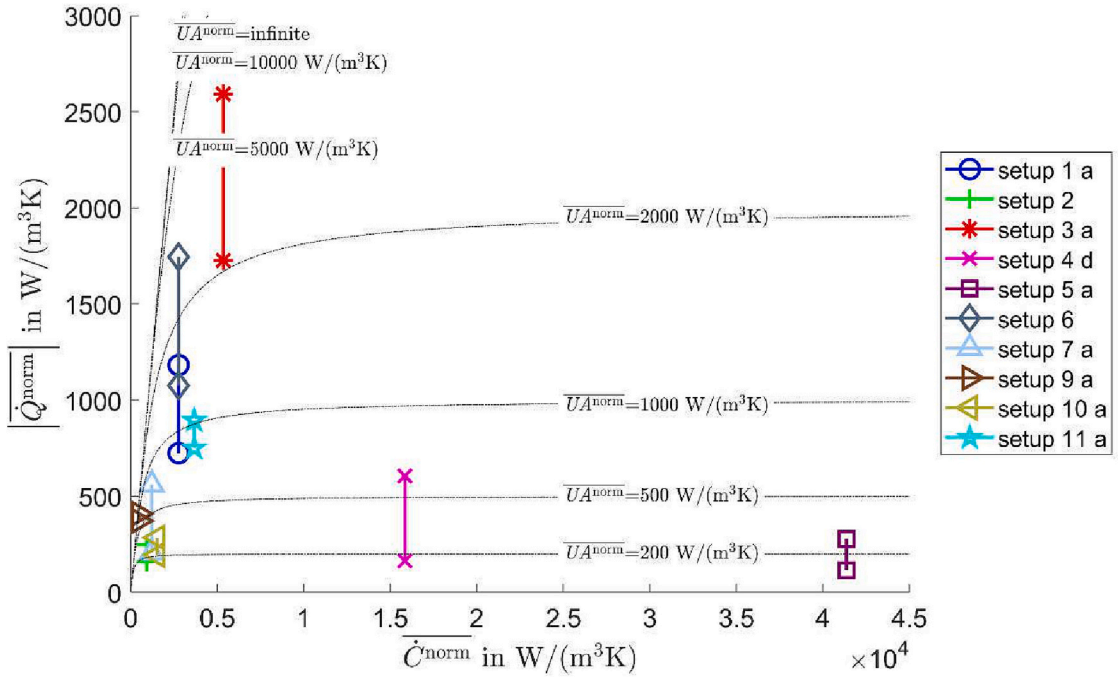

Fig. 9. $\overline{\dot{Q}^{norm}_{energy}}$ and $\overline{\dot{Q}^{norm}_{time}}$ with $T_{ref} = T_{initial}$ plotted over $\overline{\dot{C}^{norm}_{energy}}$ for one experiment of every setup except for Setup 8 – for all cases $\overline{\dot{Q}^{norm}_{energy}} > \overline{\dot{Q}^{norm}_{time}}$.

the change in $\dot{Q}^{norm}$ is less prominent for Setup 11a, resulting in a smaller $\overline{\dot{Q}^{norm}_{energy}}/\overline{\dot{Q}^{norm}_{time}}$ value. Finally, $\dot{Q}^{norm}$ is almost constant over large parts of the discharging process for Setup 9a, resulting in a $\overline{\dot{Q}^{norm}_{energy}}/\overline{\dot{Q}^{norm}_{time}}$ value close to 1.

4.1.4. Influence of V_{ref}

When performing the normalization of $\dot{Q}$ with the volume, it is important to choose a proper definition of the volume. In a final application the overall volume will matter, but for lab-scale prototypes the volume of the periphery might be unrealistically high. This can also be seen for the setups included in this study in Fig. 10, where the volume fraction of the PCM plus the HTF on the total volume varies between ~10 % and ~ 90 %. For this reason, if known, the sum of V_{PCM} and V_{HTF} is used as the reference volume throughout this study. For Setup 4 and Setup 5, this volume is not known and the sum of V_{PCM}, V_{HTF} and V_{HEX} is therefore used instead.

Empirical values, which indicate the proportion of the remaining components to the volume, are necessary to be able to draw realistic conclusions about the performance in the application. Moreover, a lab-

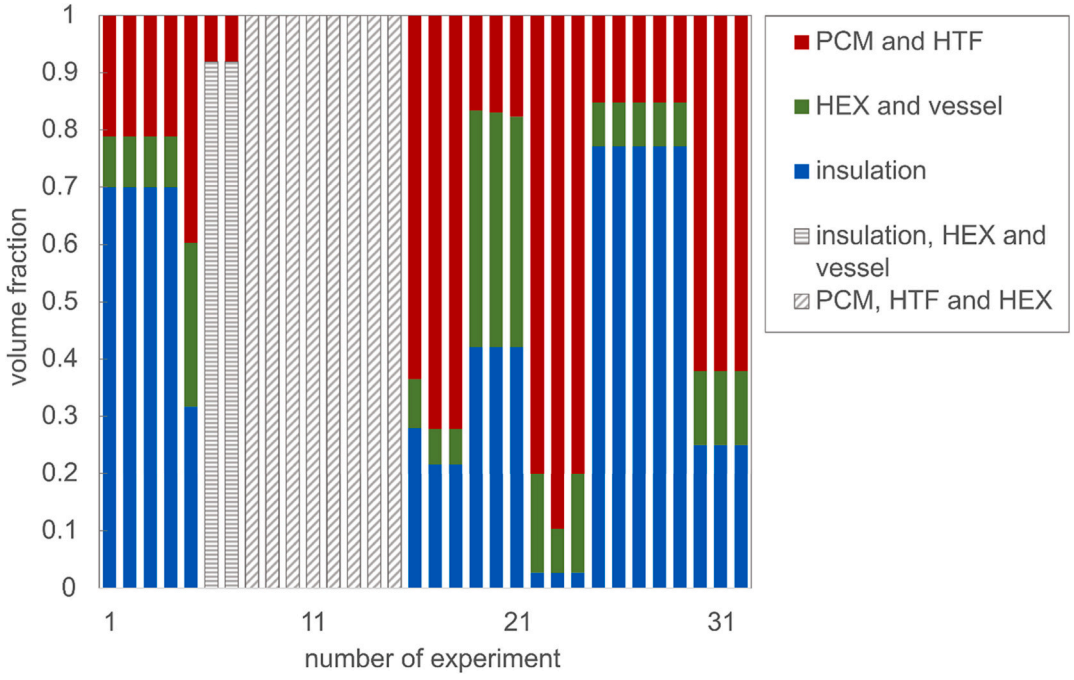

Fig. 10. Comparison of the volume fraction (of the PCM and HTF against the insulation and the HEX with vessel etc) for each experiment – for experiments 8 to 15 only the sum of the PCM, the HTF and the HEX volume is known and for experiment 6 and 7 only the PCM and HTF volume as well as the overall volume are known.

scale test might have been performed under almost adiabatic conditions, thus leading to an overestimation of the actual performance in an application. Again, future efforts should find ways to compensate for this effect.

4.2. Influence of designs, design aspects and $\overline{\dot{C}^{norm}}$

4.2.1. Influence of $\overline{\dot{C}^{norm}}$

The influence of $\overline{\dot{C}^{norm}_{energy}}$ is analyzed for $\overline{\dot{Q}^{norm}_{energy}}$ when $T_{ref} = T_{initial,}$ with the help of Fig. 11 and Fig. 12, and the outcome is compared to the results using $\overline{\dot{Q}^{norm}_{time}}$ and/or setting $T_{ref} = T_{melt,}$ which is shown in the Supplementary Material S3: Additional Results (see Fig. S3.4, see Fig. S3.5 and see Fig. S3.6). For all setups analyzed, increasing $\overline{\dot{C}^{norm}_{energy}}$ leads to a higher $\overline{\dot{Q}^{norm}_{energy}}$. This effect is stronger for LHESS with macro-encapsulated PCM (Setup 1 and Setup 7) than for the other concepts. This is due to the fact that the amount of HTF is higher for the LHESS with macro-encapsulated PCM and this leads to a longer peak in $\dot{Q}^{norm}$ in the beginning of the discharging process (see Fig. 12) – the power during this peak is directly linked to $\dot{m}$ and therefore also to $\overline{\dot{C}^{norm}_{energy}}$.

However, Setup 11 also shows a distinct increase in $\overline{\dot{Q}^{norm}_{energy}}$ for higher $\overline{\dot{C}^{norm}_{energy}}$. Interestingly, when studying $\overline{\dot{Q}^{norm}_{time}}$ instead (see Fig. S3.4 in the Supplementary Material S3: Additional Results), the influence of increasing $\overline{\dot{C}^{norm}_{energy}}$ is now somewhat lower for the LHESS with macro-encapsulated PCM, but just as prominent as for Setup 11. This can be understood better when analyzing Fig. 12 in more detail. The LHESS with macro-encapsulated PCM show the aforementioned strong peak in $\dot{Q}^{norm}$ in the beginning, which is highly influenced by $\overline{\dot{C}^{norm}_{energy}}$, but the remaining discharging process is only slightly affected due to a variation in $\overline{\dot{C}^{norm}_{energy}}$. This is different for Setup 11. Here, a much shorter peak can be seen in the beginning, but $\dot{Q}^{norm}$ is affected by changing $\overline{\dot{C}^{norm}_{energy}}$ almost throughout the entire discharging process. Now, when recalling the simple example from the Appendix D, it is clear that the energy-weighted mean value calculation has pronounced peaks stronger than a time-weighted mean value calculation. Moreover, when changing the $\overline{\dot{C}^{norm}_{energy}}$ affects the whole discharging process, this indicates that the PCM itself has a high UA value (compared to the $\overline{\dot{C}^{norm}_{energy}}$ value) leading to a high NTU.

For Setup 10, the influence of changing $\overline{\dot{C}^{norm}_{energy}}$ seems to be quite low. However, no precise statements can be made, since the effect was superimposed by random supercooling.

Finally, it should be stated that the choice of T_{ref} changed the absolute values, but had no significant impact on the effects described above.

4.2.2. Comparison of different designs

In Fig. 13, $\overline{\dot{Q}^{norm}_{energy}}$ values are plotted over $\overline{\dot{C}^{norm}_{energy}}$ for all the experiments (except for Setup 8) grouped for different designs. In Table 1, the identifiers used in Fig. 13 are explained. LHESS with a lot of liquid HTF, which are the LHESS with macro-encapsulated PCM (designs 1 and 3) show a strong dependency on $\overline{\dot{C}^{norm}_{energy}}$. The influence of $\overline{\dot{C}^{norm}_{energy}}$ on $\overline{\dot{Q}^{norm}_{energy}}$ is in general lower for designs 4–5. As expected, the LHESS with air as HTF (design 2) has a low $\overline{\dot{C}^{norm}_{energy}}$ with a somewhat lower $\overline{\dot{Q}^{norm}_{energy}}$ than most LHESS with liquid HTF. The influence of different $\overline{\dot{C}^{norm}_{energy}}$ cannot be seen for design 2, as there is only one experiment. However, it can be stated that the influence of the HTF initially in the LHESS is negligible due to the low density of air. At first glance, the LHESS with supercooled PCM (designs 3 and 5) do not show any special behavior when analyzing only the $\overline{\dot{Q}^{norm}_{energy}}$ (values)

In the Supplementary Material S3: Additional Results, in Fig. S3.7, the same results are shown including Setup 8. Moreover, also in the Supplementary Material S3: Additional Results, these results are shown for $\overline{\dot{Q}^{norm}_{time}}$ in Fig. S3.8, for $\overline{\dot{Q}^{norm}_{energy}}$ with $T_{ref} = T_{melt}$ in Fig. S3.9 and for $\overline{\dot{Q}^{norm}_{time}}$ with $T_{ref} = T_{melt}$ in Fig. S3.10. The points mentioned above do not change significantly, but one more detail can be noted. In small volume experiments where a large $\dot{m}$ is used, either for convenience or to maintain a constant wall temperature in the direction of the HTF flow,

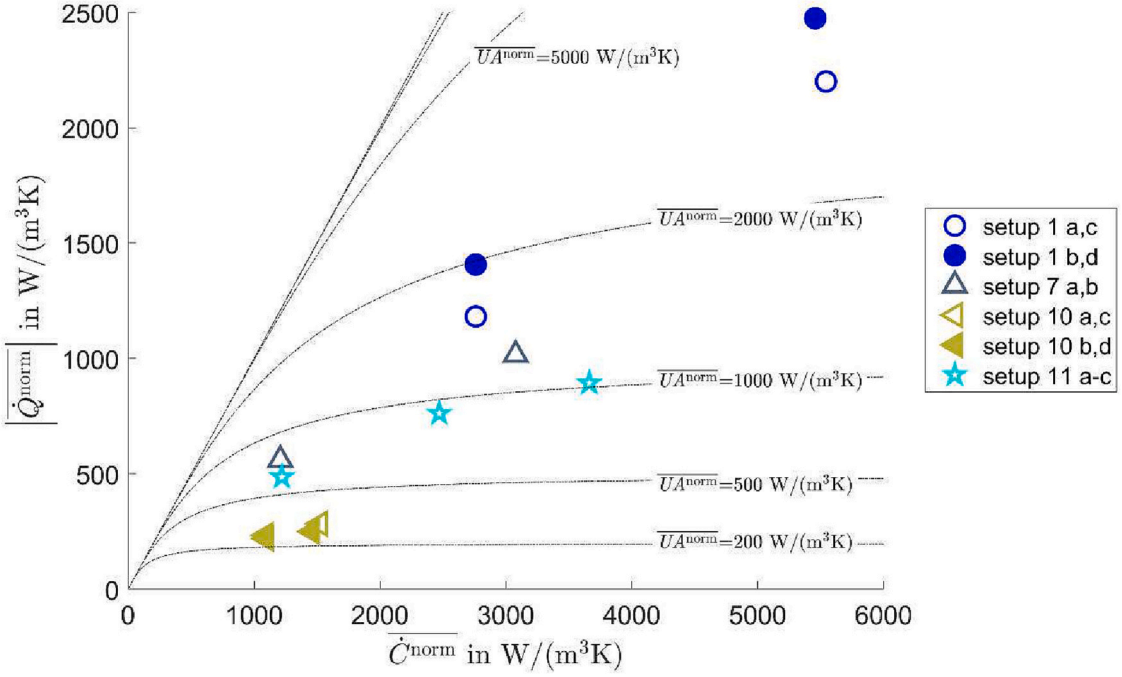

Fig. 11. $\overline{\dot{Q}^{norm}_{energy}}$ with $T_{ref} = T_{initial}$ plotted over $\overline{\dot{C}^{norm}_{energy}}$ for experiments intended to be identical but with different mass flow.

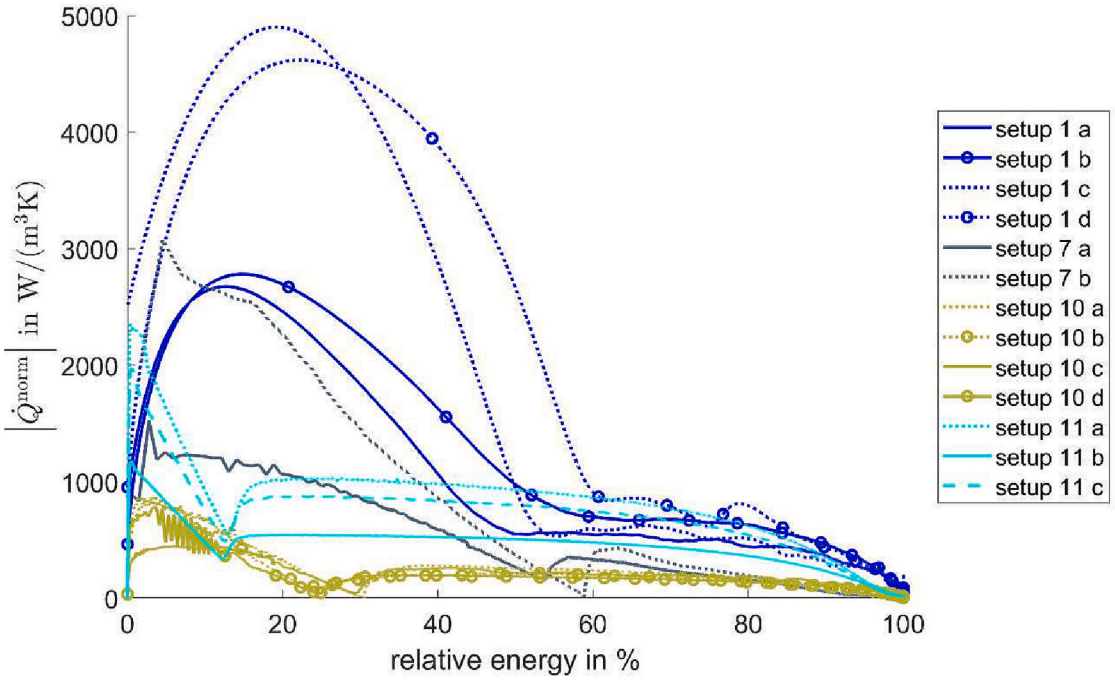

Fig. 12. $\dot{Q}^{norm}$ with $T_{ref} = T_{initial}$ plotted over relative energy for experiments intended to be identical but with different mass flow.

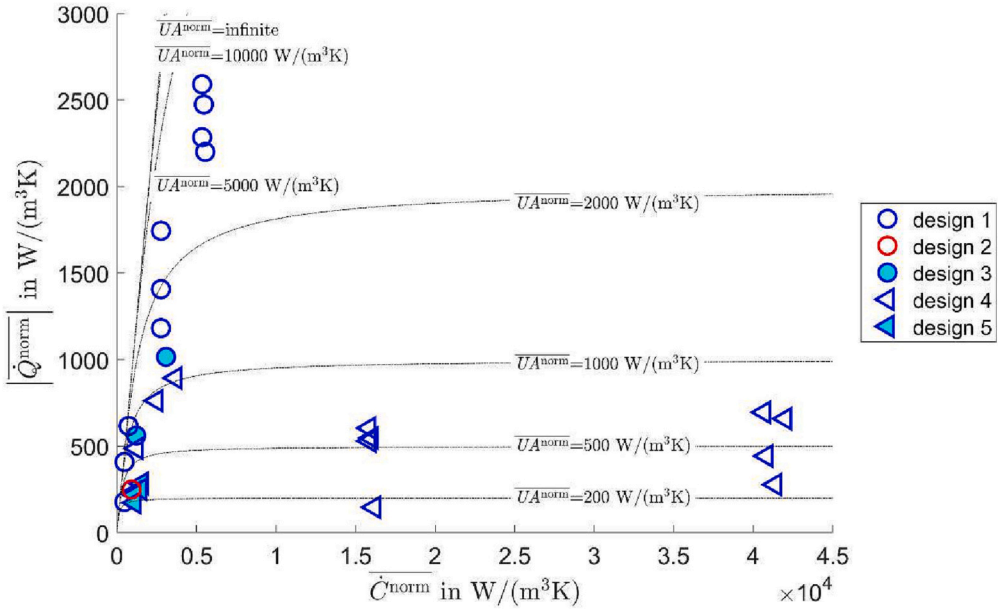

Fig. 13. $\overline{\dot{Q}^{norm}_{energy}}$ with $T_{ref} = T_{initial}$ plotted over $\overline{\dot{C}^{norm}_{energy}}$ (for all experiments except the ones of Setup 8) categorized by the design.

unrealistically high $\overline{\dot{C}^{norm}_{energy}}$ values result for real scale applications and the diagram becomes somewhat unclear. For instance, $\dot{m}$ applied for Setup 8, which refers to design 6, is equivalent to almost 1400 $\frac{kg}{m^3 \bullet min}$ when the volume of the HTF plus the PCM is used as reference.

4.2.3. Variation of design aspects

In Fig. 14, $\overline{\dot{Q}^{norm}_{energy}}$ values are plotted over $\overline{\dot{C}^{norm}_{energy}}$ for all experiments with setups where a variation in the design was performed. For all setups, the variations of the designs result in a large change in $\overline{\dot{Q}^{norm}_{energy}}$, and for 3 setups, the results follow the intuition – more coils (Setup 4), more fins (Setup 5) and (longer) fins (Setup 8) lead to higher $\overline{\dot{Q}^{norm}_{energy}}$ values. For Setup 9, this basic check cannot be performed as the design does not change in such a simple way. In general, using $\overline{\dot{Q}^{norm}_{time}}$ and/or $T_{ref} = T_{melt}$ instead (see Fig. S3.11, Fig. S3.12 and Fig. S3.13 in the Supplementary Material S3: Additional Results) does not change the order of $\overline{\dot{Q}^{norm}_{energy}}$ or $\overline{\dot{Q}^{norm}_{time}}$ for the variations, but using $\overline{\dot{Q}^{norm}_{time}}$ instead of $\overline{\dot{Q}^{norm}_{energy}}$ may have a distinct effect on the difference between two variations.

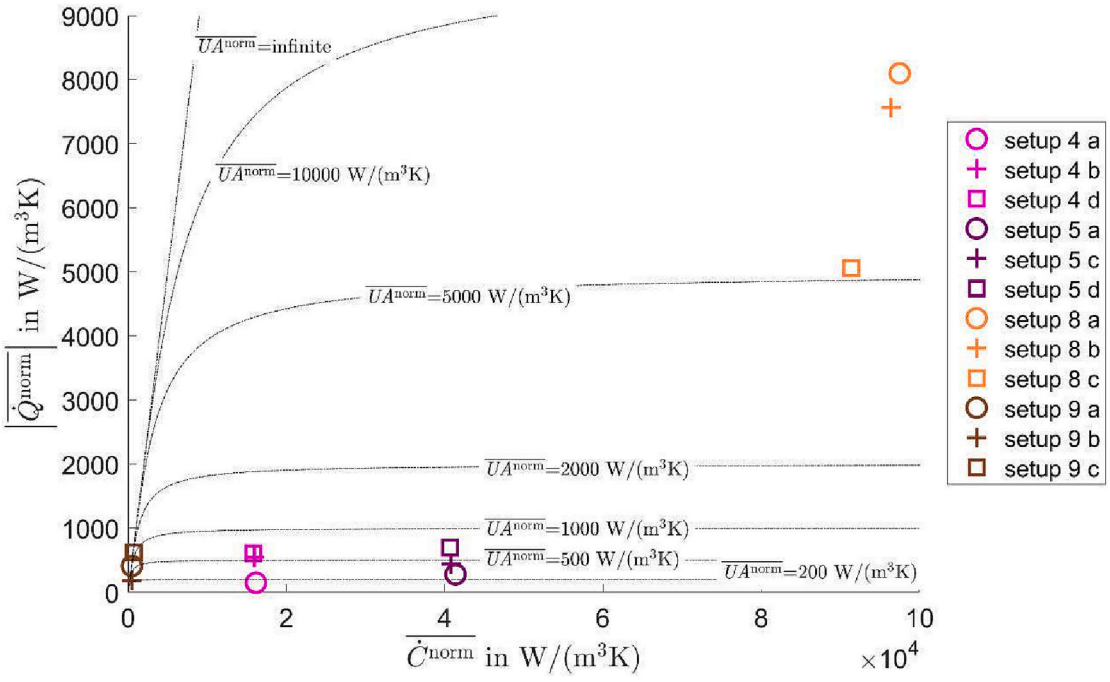

Fig. 14. $\overline{\dot{Q}^{\mathrm{norm}}_{\mathrm{energy}}}$ with $T_{ref} = T_{initial}$ plotted over $\overline{\dot{C}^{\mathrm{norm}}_{\mathrm{energy}}}$ for experiments intended to be identical but with variations in the design.

5. Conclusion

A method for comparing the discharging process (solidification) of LHESS with different designs and sizes and under different boundary and initial conditions was analyzed with the help of experimental results from eleven setups and further developed in this paper. The main idea of the approach is to normalize $\dot{Q}$ by the volume and a reference temperature difference, calculate a mean value and present the results plotted over a normalized mean value of the capacity flow in a so-called $\overline{\dot{C}^{norm}}/\overline{\dot{Q}^{norm}}$-plot. The approach allows us to compare a fairly large amount of results from very different LHESS, only very high mass flow rates for small scale experiments caused problems in the presentation. However, a major open question is how fair such a comparison is. In particular, the issue of how the choice of the reference temperature – melting and initial temperature – for normalization and the type of mean value calculation of $\dot{Q}$ – time-weighted or energy-weighted – influences the results has been addressed.

With regard to the reference temperatures, the cases where large differences between the two possibilities exist and where comparable results are achieved were shown. Moreover, it was concluded that neither choice of the reference temperatures can give fully fair results for the sensible and latent heat parts. To overcome this drawback, the possibility of weighting the reference temperature in the mean value calculation according to the latent and sensible parts was mentioned and should be studied in the future.

With respect to the mean value calculation, it was found that the time-weighted calculation is highly dependent on the stopping criterion. This is not true for the energy-weighted mean value. However, unlike the time-weighted calculation, there is no easy way to interpret the physical meaning for the energy-weighted mean value calculation. In addition, the energy-weighted mean value tends to overweight peaks in $\dot{Q}$. Irrespective of the choice of the mean value calculation, the information on the slope of $\dot{Q}$ during the discharging process gets lost due to the averaging. An option to overcome this drawback is to compare the energy-weighted with the time-weighted $\dot{Q}$ value. Analyzing the experimental results in this study, it would seem that the larger the difference between both mean values, the more $\dot{Q}$ changes during the discharging process. Thus, more extensive tests or calculations need to be done to investigate this further.

The effect of the reference volume on $\dot{Q}^{norm}$ is linear and therefore straightforward. Nevertheless, the selection of the reference volume is not trivial, since the share of the different volumes in the total volume depends on the size of LHESS. Since, in this work, not all volume fractions of all setups are known, the reference volume for most LHESS was set to the sum of V_{PCM} and V_{HTF} and, for the other two setups, to the sum of V_{PCM}, V_{HTF} and V_{HEX}. Future efforts should address the question of how the proportion of the different volumes changes with the size.

Finally, it can be stated that reasonable results can be obtained with each variant studied, but they are always somewhat subject to limitations and biases. Therefore, it is essential to be aware of these in the application and to clearly indicate the choice of the reference temperature and volume and the method for calculating the mean value.

Future work should focus on the points addressed regarding the mean value calculation and the normalization. Moreover, measures will need to be adopted when the approach is applied to the charging process (melting) of LHESS, as convection may play a major role and, in consequence, the heat transfer rate is no longer linearly dependent on the temperature difference. The authors themselves will continue their work under Subtask E of the recently launched IEA SHC Task 67/ES Task 40. Finally, it should be remembered that the power rate is only one of several important aspects defining an LHESS and showing $\dot{Q}$ in a normalized way neglects, for instance, the energy density of the storage. Thus, future efforts should therefore also deal with the integration of energy density into the approach and investigate combinations with methods to study the cost-effectiveness [49].

CRediT authorship contribution statement

Andreas König-Haagen: Conceptualization, Methodology, Software, Validation, Investigation, Resources, Data curation, Writing – original draft, Writing – review & editing, Visualization. **Stephan Höhlein:** Conceptualization, Validation, Investigation, Resources, Data curation, Writing – review & editing. **Ana Lázaro:** Conceptualization, Methodology, Validation, Investigation, Resources, Data curation, Writing – review & editing. **Mónica Delgado:** Conceptualization,

Validation, Investigation, Resources, Data curation, Writing – review & editing. **Gonzalo Diarce:** Conceptualization, Validation, Investigation, Resources, Data curation, Writing – review & editing. **Dominic Groulx:** Conceptualization, Validation, Investigation, Resources, Data curation, Writing – review & editing. **Florent Herbinger:** Conceptualization, Validation, Investigation, Resources, Data curation, Writing – review & editing. **Ajinkya Patil:** Conceptualization, Validation, Investigation, Resources, Data curation, Writing – review & editing. **Gerald Englmair:** Conceptualization, Validation, Investigation, Resources, Data curation, Writing – review & editing. **Gang Wang:** Conceptualization, Validation, Investigation, Resources, Data curation, Writing – review & editing. **Amir Abdi:** Conceptualization, Validation, Investigation, Resources, Data curation, Writing – review & editing. **Justin N.W. Chiu:** Conceptualization, Validation, Investigation, Resources, Data curation, Writing – review & editing. **Tianhao Xu:** Conceptualization, Validation, Investigation, Resources, Data curation, Writing – review & editing. **Christoph Rathgeber:** Conceptualization, Validation, Investigation, Resources, Data curation, Writing – review & editing. **Simon Pöllinger:** Conceptualization, Validation, Investigation, Resources, Data curation, Writing – review & editing. **Stefan Gschwander:** Conceptualization, Validation, Investigation, Resources, Data curation, Writing – review & editing. **Sebastian Gamisch:** Conceptualization, Validation, Investigation, Resources, Data curation, Writing – review & editing.

Declaration of competing interest

The authors declare that they have no known competing financial interests or personal relationships that could have appeared to influence the work reported in this paper.

Data availability

Data will be made available on request.

Acknowledgments

Andreas König-Haagen is grateful for the financial support of the Deutsche Forschungsgemeinschaft, (DFG, German Research Foundation) under Grant no KO 6286/1-1.

The authors of Fraunhofer ISE acknowledge the financial support from the German Federal Ministry for Economic Affair and Energy (BMWi) for the Prolatent Project (FKZ 0325549A).

The work of DTU was supported by the Danish Energy Agency through the EUDP program.

The work of ZAE Bayern is part of the projects properPCM and AMThES and was supported by the German Federal Ministry of Economic Affairs and Energy under the project codes 03ET1342A and 03EN6006, respectively.

Appendix A. List of experiments and setups

Table A.1
List of experiments and setups.

Name	Ref.	Design	V_{PCM}	V_{HTF}	V_{HEX}	V_{INS}	V_{TOT}	PCM	T_{melt}	HTF	$T_{initial}$	T_{inlet}	$\dot{m}$
Units	–	–	m^3	m^3	m^3	m^3	m^3	–	°C	–	°C	°C	$\frac{kg}{s}$
Setup 1a	[37]	1	0.014	0.018	0.014	0.106	0.152	Magnesium chloride hexahydrate	115.1	Oil	128	108	0.0414
Setup 1b	[37]	1	0.014	0.018	0.014	0.106	0.152	Magnesium chloride hexahydrate	115.1	Oil	133	103	0.0415
Setup 1c	[37]	1	0.014	0.018	0.014	0.106	0.152	Magnesium chloride hexahydrate	115.1	Oil	129	108	0.0833
Setup 1d	[37]	1	0.014	0.018	0.014	0.106	0.152	Magnesium chloride hexahydrate	115.1	Oil	134	102	0.0821
Setup 2	[28]	2	0.17	0.31	0.34	0.38	1.2	RT27	26–28	Air	40	16	0.430
Setup 3a	[27]	1	0.0200	0.011	0.347		0.378	RT60	57	Water	60	45	0.0390
Setup 3b	[27]	1	0.0200	0.0105	0.3475		0.3780	RT60	57	Water	65	51	0.0390
Setup 4a 1 coil	[43]	4	0.014			–	–	Dodecanoic Acid	43.3 ± 1.5	Water	65	21	0.0550
Setup 4b 2 coils	[43]	4	0.014			–	–	Dodecanoic Acid	43.3 ± 1.5	Water	65	21	0.0550
Setup 4c 3 coils	[43]	4	0.014			–	–	Dodecanoic Acid	43.3 ± 1.5	Water	55	21	0.0550
Setup 4d 3 coils	[43]	4	0.014			–	–	Dodecanoic Acid	43.3 ± 1.5	Water	65	21	0.0550
Setup 5a 4 finned tubes	[23]	4	0.0137			–	–	Dodecanoic Acid	43.3 ± 1.5	Water	63	22	0.134
Setup 5b 8 finned tubes	[23]	4	0.0137			–	–	Dodecanoic Acid	43.3 ± 1.5	Water	54	32	0.137
Setup 5c 8 finned tubes	[23]	4	0.0137			–	–	Dodecanoic Acid	43.3 ± 1.5	Water	64	25	0.132
Setup 5d 12 finned tubes	[23]	4	0.0137			–	–	Dodecanoic Acid	43.3 ± 1.5	Water	64	26	0.134
Setup 6	[45,46]	1	0.104	0.075	0.024	0.079	0.282	Sodium acetate trihydrate composite	57	Water	91	30	0.118

(*continued on next page*)

Table A.1 (*continued*)

Name	Ref.	Design	V_{PCM}	V_{HTF}	V_{HEX}	V_{INS}	V_{TOT}	PCM	T_{melt}	HTF	$T_{initial}$	T_{inlet}	$\dot{m}$
Units	–	–	m^3	m^3	m^3	m^3	m^3	–	°C	–	°C	°C	$\frac{kg}{s}$
Setup 7a	[47]	3	0.158	0.059	0.019	0.065	0.301	Sodium acetate trihydrate composite	58	Water	90	25	0.0622
Setup 7b	[47]	3	0.158	0.059	0.019	0.065	0.301	Sodium acetate trihydrate composite	58	Water	88	28	0.159
Setup 8a Long fins	[29]	6	5.9e-04	1.17e-04	0.00176	0.00179	0.00425	n-eicosane	36.4	Water	60	16	0.0164
Setup 8b Mid-way fins	[29]	6	6.05e-04	1.17e-04	0.00174	0.00179	0.00425	n-eicosane	36.4	Water	60	15	0.0166
Setup 8c No fins	[29]	6	6.35e-04	1.17e-04	0.00171	0.00179	0.00425	n-eicosane	36.4	Water	60	15	0.0165
Setup 9a Slab encapsulation		1	0.078	0.300	0.082	0.013	0.477	ATP60	60–62	Water	72	47	0.0427
Setup 9b Spiral coil		1	0.520	0.020	0.045	0.015	0.580	Crodatherm60	59–60	Water	72	46	0.0553
Setup 9c Ellipsoid encapsulation	[50]	1	0.078	0.300	0.082	0.013	0.477	ATP60	60–62	Water	72	46	0.0660
Setup 10a	[51]	5	0.034	0.009	0.022	0.218	0.283	Erythritol	119	Oil Therminol 66	139	100	0.0350
Setup 10b	[51]	5	0.034	0.009	0.022	0.218	0.283	Erythritol	119	Oil Therminol 66	134	105	0.0333
Setup 10c	[51]	5	0.034	0.009	0.022	0.218	0.283	Erythritol	119	Oil Therminol 66	139	101	0.0250
Setup 10d	[51]	5	0.034	0.009	0.022	0.218	0.283	Erythritol	119	Oil Therminol 66	134	105	0.0250
Setup 10e	[51]	5	0.034	0.009	0.022	0.218	0.283	Erythritol	119	Oil Therminol 66	129	110	0.0250
Setup 11a	[52,53]	4	0.93	0.02	0.20	0.38	1.54	calcium chloride hexahydrate	29	Water	36	22	0.837
Setup 11b	[52,53]	4	0.93	0.02	0.20	0.38	1.54	Calcium chloride Hexahydrate	29	Water	36	22	0.279
Setup 11c	[52,53]	4	0.93	0.02	0.20	0.38	1.54	Calcium chloride hexahydrate	29	Water	36	22	0.558

Appendix B. Discussion based on $\dot{Q}^{norm}$ plotted over relative energy

Description of several aspects of the results presented in Fig. 3:

- Setup 1a: the experiment was performed using an LHESS with macro-encapsulated PCM and a large amount of liquid HTF. This results in a peak in $\dot{Q}^{norm}$ at the beginning that lasts until approximately 50 % of the total energy is discharged. Afterwards, the heat transfer is limited mostly by the heat conduction in the PCM.
- Setup 3a: the experiment was also performed using an LHESS with macro-encapsulated PCM and a large amount of liquid HTF. This results in a high $\dot{Q}^{norm}$ at the beginning, but unlike in Setup 1a, no clear peak can be seen. The reason for this might be the mixing of the HTF or a rather low amount of PCM in the LHESS.
- Setup 2: the experiment uses air as HTF. This leads to a high heat transfer resistance between the HTF and the PCM containers. This resistance seems to dominate the overall process and leads to an almost constant $\dot{Q}^{norm}$ until about 60 % of the energy is discharged. Also, the HTF has a very low $\dot{C}^{norm}$ and therefore no peak due to the HTF is seen at the beginning.
- Setup 4d: the experiment applies a small amount of liquid HTF and has a high $\dot{C}^{norm}$ value. Therefore, at the beginning, a very high but short peak in $\dot{Q}^{norm}$ can be seen. Afterwards, the heat transfer seems to be limited by the heat transfer (conduction and convection) in the PCM and the result is a reduced $\dot{Q}^{norm}$.
- Both Setup 6 and 10: the experiments show the characteristic behavior of LHESS with supercooled PCM. First, the sensible heat of the liquid PCM is extracted with a rather high $\dot{Q}^{norm}$ rate – the heat transfer is supported by natural convection in the liquid PCM. Then, after a minimum in $\dot{Q}^{norm}$, the solidification starts and the power increases again. While in Setup 10a, about 30 % of the energy is discharged before the solidification starts, it is more than 50 % for Setup 6.

Appendix C. Theoretical discussion on the influence of T_{ref}

In order to obtain a uniform terminology and to describe possible effects of the choice of T_{ref}, different constellations of $T_{initial}$, T_{inlet} and T_{melt} are illustrated in Fig. C.1. For simplicity, it is assumed that the material properties are constant. The temperatures in examples 1 and 2 are seen as symmetrical and that of examples 3 and 4 as unsymmetrical. Three cases are now discussed briefly:

i) comparing example 1 with example 2
ii) comparing example 1 with example 4
iii) comparing example 3 with example 4

For case i), $(T_{initial} - T_{inlet})/(T_{melt} - T_{inlet})$ is identical in both examples. Such a change in the boundary and initial conditions for temperature will be referred to as proportional. In case ii), this is no longer true as $\left(T_{melt}^{exp1} - T_{inlet}^{exp1}\right) = \left(T_{melt}^{exp4} - T_{inlet}^{exp4}\right)$, but $\left(T_{initial}^{exp1} - T_{inlet}^{exp1}\right) \rangle \left(T_{initial}^{exp4} - T_{inlet}^{exp4}\right)$. The same holds for case iii), as $\left(T_{initial}^{exp3} - T_{inlet}^{exp3}\right) = \left(T_{initial}^{exp4} - T_{inlet}^{exp4}\right)$, but $\left(T_{melt}^{exp3} - T_{inlet}^{exp3}\right) \langle \left(T_{melt}^{exp4} - T_{inlet}^{exp4}\right)$. Such a change in the boundary and initial conditions for temperature will be referred to as not proportional.

In other words, in each way, the sensible or the latent heat is weighted incorrectly, depending on whether T_{melt} or $T_{initial}$ is used. However, in case i), this error is inherently the same for the sensible and the latent heat for both examples (e.g., if in example 1 the latent heat is weighted with a temperature difference that is 50 % wrong, this also holds for example 2). In cases ii) and iii), this is no longer true, making a comparison even more difficult. Finally, it should be mentioned that even for proportional temperature conditions, unfair results are expected when the Ste is significantly different.

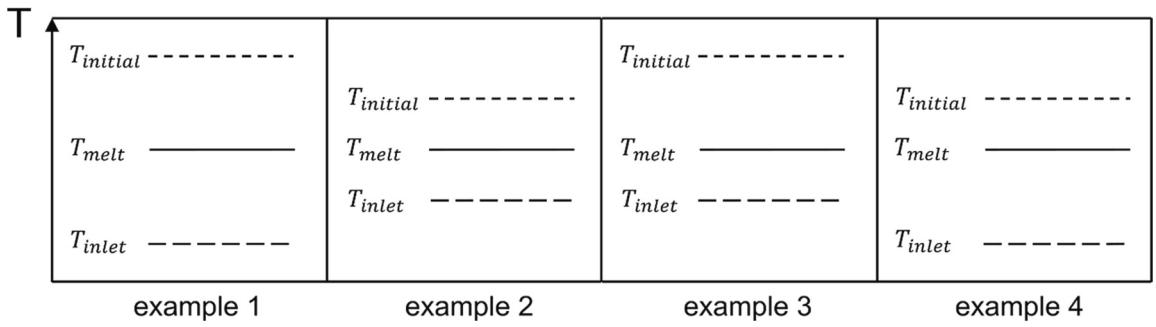

Fig. C.1. Comparison of different examples for boundary and initial conditions of temperature.

In Table C.1, $(T_{initial} - T_{inlet})/(T_{melt} - T_{inlet})$ is given for all experiments that have a variation in the boundary and initial conditions of temperature with otherwise intended identical conditions. Note that $(T_{initial} - T_{inlet})/(T_{melt} - T_{inlet}) = 2$ implies symmetrical conditions and the closer $(T_{initial} - T_{inlet})/(T_{melt} - T_{inlet})$ is to 1, the smaller the expected difference between the two choices for T_{ref}.

Table C.1
Overview of $(T_{initial} - T_{inlet})/(T_{melt} - T_{inlet})$ for experiments with different boundary and initial conditions of temperature.

Experiment	Compared to	$(T_{initial} - T_{inlet})/(T_{melt} - T_{inlet})$
Setup 1a	Setup 1b	2.817
Setup 1b	Setup 1a	2.479
Setup 1c	Setup 1d	2.958
Setup 1d	Setup 1c	2.443
Setup 3a	Setup 3b	1.250
Setup 3b	Setup 3a	2.333
Setup 4c	Setup 4d	1.525
Setup 4d	Setup 4c	1.973
Setup 5b	Setup 5c	2
Setup 5c	Setup 5b	2.167
Setup 10a	Setup 10b	2.053
Setup 10b	Setup 10a	2.071
Setup 10c	Setup 10d	2.111
Setup 10d	Setup 10c	2.071

Appendix D. Theoretical discussion on the mean value calculation

In Fig. D.1, $\overline{\dot{Q}_{energy}^{norm}}$ and $\overline{\dot{Q}_{time}^{norm}}$ are plotted over relative energy (the beginning of the integration was fixed at the start of the experiment, but the end was varied between 90 % and 100 %) for chosen experiments. It is noticeable that $\overline{\dot{Q}_{energy}^{norm}}$ is always larger than $\overline{\dot{Q}_{time}^{norm}}$ and that $\overline{\dot{Q}_{time}^{norm}}$ changes strongly towards the end of the discharging process. From a theoretical perspective, $\overline{\dot{Q}_{time}^{norm}}$ even approaches zero for a full discharge as the amount of heat to be transferred is fixed, but the time to completely discharge or charge an LHESS is infinite in most cases (for an ideal direct storage, for instance, this is not

the situation). On the contrary, $\overline{\dot{Q}^{norm}_{energy}}$ only changes very slightly towards the end of the discharging process. This is an advantage, as an exact determination of the state of charge is often not possible and an error of just a few percent in the relative energy may lead to large deviations in $\overline{\dot{Q}^{norm}_{time}}$ but not in $\overline{\dot{Q}^{norm}_{energy}}$. However, $\overline{\dot{Q}^{norm}_{time}}$ allows the time needed for discharging to be directly calculated, whereas such an easy to interpret and useful physical meaning has not been found so far for $\overline{\dot{Q}^{norm}_{energy}}$. Moreover, $\overline{\dot{Q}^{norm}_{energy}}$ may privilege LHESS with peaks in $\dot{Q}^{norm}$, which can be explained using the two simple examples shown in Fig. D.2. For the sake of simplicity, it is assumed that both tests were carried out under identical conditions and with the same volume, which is why no normalization is required in this case. Example a corresponds to an LHESS with a constant $\dot{Q}$ of 10 kW and example b reflects an LHESS in which $\dot{Q}$ is 15 kW for the first half of the discharge time and 5 kW for the second half. When $\dot{Q}$ of the same examples is plotted over energy (see the right side of Fig. D.2), the slope of $\dot{Q}$ does not change for example a, but it does for example b; − 75 % of the energy is discharged with a $\dot{Q}$ of 15 kW and the remaining 25 % is discharged with a $\dot{Q}$ of 5 kW. Obviously, $\overline{\dot{Q}_{time}}$ is 10 kW for both examples, but $\overline{\dot{Q}_{energy}}$ is 10 kW for example a and 12.5 kW for example b. Generally speaking, the $\dot{Q}$ curve of example a is likely to be preferred for most applications. In conclusion, for the energy-weighted calculation, a more likely unwanted slope of the $\dot{Q}$ curve gives higher $\overline{\dot{Q}_{energy}}$ values than a constant $\dot{Q}$. Finally, it must be noted that, regardless of the procedure for the mean value calculation, the information on the slope of the $\dot{Q}$ curve is lost.

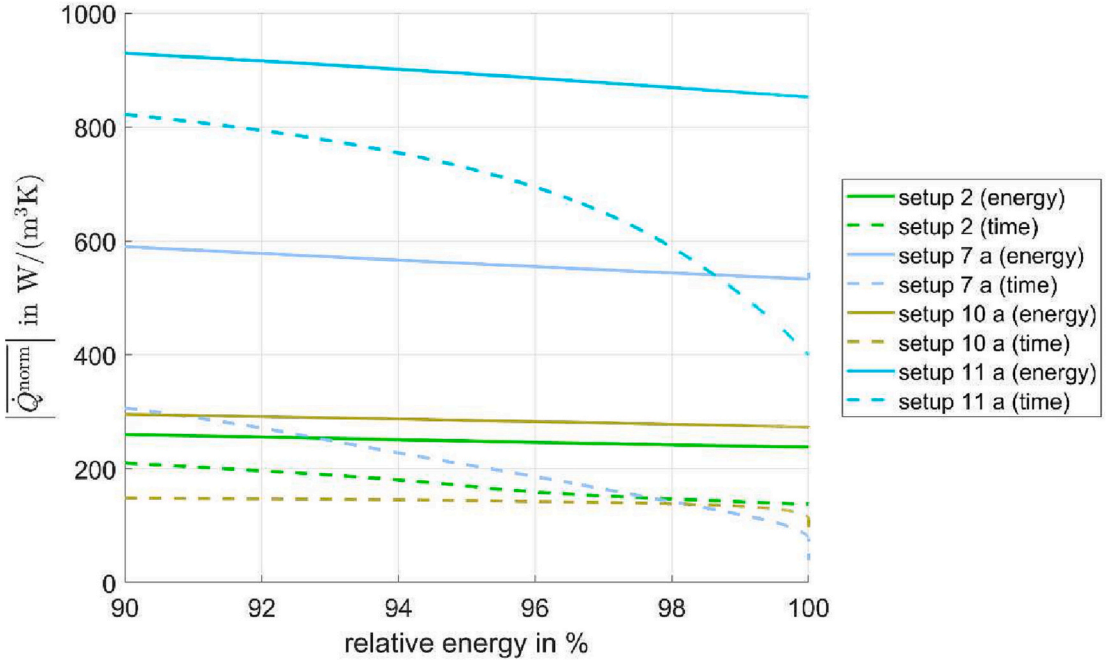

Fig. D.1. $\overline{\dot{Q}^{norm}_{energy}}$ and $\overline{\dot{Q}^{norm}_{time}}$ with $T_{ref} = T_{initial}$ plotted over relative energy for chosen experiments.

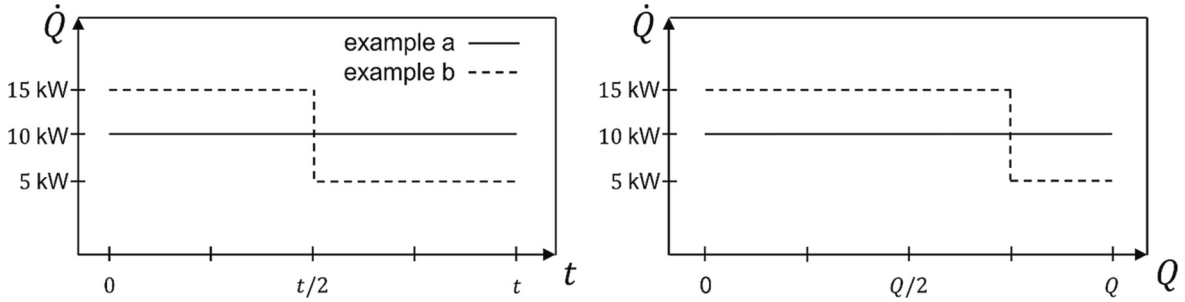

Fig. D.2. Two simple examples for $\dot{Q}$ plotted over time (left) and energy (right).

Appendix E. Supplementary data

Supplementary data to this article can be found online at https://doi.org/10.1016/j.est.2023.108428.

References

[1] D. Groulx, The rate problem in solid-liquid phase change heat transfer: efforts and questions towards heat exchanger design rules, in: Proceedings of the 16th International Heat Transfer Conference. 16th International Heat Transfer Conference, Beijing, China, August 10–15, 2018, 2018.

[2] S. Ebadi, S.H. Tasnim, A.A. Aliabadi, S. Mahmud, Melting of nano-PCM inside a cylindrical thermal energy storage system: Numerical study with experimental

verification, Energy Conversion and Management 166 (2018) 241–259, https://doi.org/10.1016/j.enconman.2018.04.016.
[3] R. Siegel, Solidification of low conductivity material containing dispersed high conductivity particles, International Journal of Heat and Mass Transfer 20 (1977) 1087–1089, https://doi.org/10.1016/0017-9310(77)90195-8.
[4] M. Dannemand, J.B. Johansen, S. Furbo, Solidification behavior and thermal conductivity of bulk sodium acetate trihydrate composites with thickening agents and graphite, Solar Energy Materials and Solar Cells 145 (2016) 287–295, https://doi.org/10.1016/j.solmat.2015.10.038.
[5] D. Singh, W. Yu, W. Zhao, T. Kim, D.M. France, R.K. Smith, Development and prototype testing of MgCl2/graphite foam latent heat thermal energy storage system, Solar Energy 159 (2018) 270–282, https://doi.org/10.1016/j.solener.2017.10.084.
[6] R. Srikanth, P. Nemani, C. Balaji, Multi-objective geometric optimization of a PCM based matrix type composite heat sink, Applied Energy 156 (2015) 703–714, https://doi.org/10.1016/j.apenergy.2015.07.046.
[7] X. Tong, J.A. Khan, M. RuhulAmin, Enhancement of heat transfer by inserting a metal matrix into a phase change material, Numerical Heat Transfer, Part A: Applications 30 (1996) 125–141, https://doi.org/10.1080/10407789608913832.
[8] A. Mills, M. Farid, J.R. Selman, S. Al-Hallaj, Thermal conductivity enhancement of phase change materials using a graphite matrix, Applied Thermal Engineering 26 (2006) 1652–1661, https://doi.org/10.1016/j.applthermaleng.2005.11.022.
[9] M. Yuan, Y. Ren, C. Xu, F. Ye, X. Du, Characterization and stability study of a form-stable erythritol/expanded graphite composite phase change material for thermal energy storage, Renewable Energy 136 (2019) 211–222, https://doi.org/10.1016/j.renene.2018.12.107.
[10] H. Mehling, S. Hiebler, Ziegler, F. Latent heat storage using a PCM-graphite composite material, Proceedings of TERRASTOCK, 2000.
[11] S. Höhlein, A. König-Haagen, D. Brüggemann, Macro-Encapsulation of Inorganic Phase-Change Materials (PCM) in Metal Capsules, Materials 11 (2018) 1752, https://doi.org/10.3390/ma11091752.
[12] A.F. Regin, S.C. Solanki, J.S. Saini, Heat transfer characteristics of thermal energy storage system using PCM capsules: a review, RENEW SUST ENERG REV 12 (2008) 2438–2458.
[13] D. Groulx, P.H. Biwole, M. Bhouri, Phase change heat transfer in a rectangular enclosure as a function of inclination and fin placement, International Journal of Thermal Sciences 151, 106,260 (2020), https://doi.org/10.1016/j.ijthermalsci.2020.106260.
[14] R. Velraj, R.V. Seeniraj, B. Hafner, C. Faber, K. Schwarzer, Heat transfer enhancement in a latent heat storage system, Solar Energy 65 (1999) 171–180, https://doi.org/10.1016/S0038-092X(98)00128-5.
[15] V.H. Morcos, Investigation of a latent heat thermal energy storage system, Solar & Wind Technology 7 (1990) 197–202.
[16] S. Kuboth, A. König-Haagen, D. Brüggemann, Numerical analysis of shell-and-tube type latent thermal energy storage performance with different arrangements of circular fins, Energies 10 (2017) 274, https://doi.org/10.3390/en10030274.
[17] W.R. Humphries, E.I. Griggs, A design handbook for phase change thermal control and energy storage devices, National Aeronautics and Space Administration, Scientific and Technical Information Office, 1977.
[18] S. Gamisch, S. Gschwander, S.J. Rupitsch, Numerical and experimental investigation of wire cloth heat exchanger for latent heat storages, Energies 14 (2021) 7542, https://doi.org/10.3390/en14227542.
[19] N.I. Ibrahim, F.A. Al-Sulaiman, S. Rahman, B.S. Yilbas, A.Z. Sahin, Heat transfer enhancement of phase change materials for thermal energy storage applications: a critical review, RENEW SUST ENERG REV 74 (2017) 26–50, https://doi.org/10.1016/j.rser.2017.01.169.
[20] S. Jegadheeswaran, S.D. Pohekar, Performance enhancement in latent heat thermal storage system: a review, RENEW SUST ENERG REV 13 (2009) 2225–2244.
[21] Z. Khan, Z. Khan, A. Ghafoor, A review of performance enhancement of PCM based latent heat storage system within the context of materials, thermal stability and compatibility, Energy Conversion and Management 115 (2016) 132–158, https://doi.org/10.1016/j.enconman.2016.02.045.
[22] S. Jegadheeswaran, A. Sundaramahalingam, S.D. Pohekar, Alternative heat transfer enhancement techniques for latent heat thermal energy storage system: a review, Int J Thermophys 42 (2021) 1–48, https://doi.org/10.1007/s10765-021-02921-x.
[23] Herbinger, F.; Patil, A.; Groulx, D. Characterization of Different Geometrical Variations of a Vertical Finned Tube-and-Shell Heat Exchanger. In *Eurotherm Seminar #112*, Advances in Thermal Energy Storage, 2019.
[24] V. Saydam, M. Parsazadeh, M. Radeef, X. Duan, Design and experimental analysis of a helical coil phase change heat exchanger for thermal energy storage, Journal of Energy Storage 21 (2019) 9–17, https://doi.org/10.1016/j.est.2018.11.006.
[25] L. Kalapala, J.K. Devanuri, Influence of operational and design parameters on the performance of a PCM based heat exchanger for thermal energy storage – a review, Journal of Energy Storage 20 (2018) 497–519, https://doi.org/10.1016/j.est.2018.10.024.
[26] D. Groulx, A. Castell, C. Solé, Design of latent heat energy storage systems using phase change materials, *Advances in Thermal Energy Storage Systems*; Elsevier (2021) 331–357.
[27] P. Larrinaga, G. Diarce, Á. Campos-Celador, A. García-Romero, Parametric characterization of a full-scale plate-based latent heat thermal energy storage system, Applied Thermal Engineering 178 (2020) 115–441, https://doi.org/10.1016/j.applthermaleng.2020.115441.
[28] P. Dolado, A. Lazaro, J.M. Marin, B. Zalba, Characterization of melting and solidification in a real-scale PCM–air heat exchanger: experimental results and empirical model, Renewable Energy 36 (2011) 2906–2917, https://doi.org/10.1016/j.renene.2011.04.008.
[29] A. Abdi, M. Shahrooz, J.N.W. Chiu, V. Martin, Experimental investigation of solidification and melting in a vertically finned cavity, Applied Thermal Engineering 198 (2021) 117,459, https://doi.org/10.1016/j.applthermaleng.2021.117459.
[30] K. Ismail, M.M. Gonçalves, Thermal performance of a pcm storage unit, Energy Conversion and Management 40 (1999) 115–138, https://doi.org/10.1016/S0196-8904(98)00042-9.
[31] M. Belusko, E. Halawa, F. Bruno, Characterising PCM thermal storage systems using the effectiveness-NTU approach, International Journal of Heat and Mass Transfer 55 (2012) 3359–3365.
[32] N. Shamsundar, R. Srinivasan, Effectiveness-NTU charts for heat recovery from latent heat storage units, J. Sol. Energy Eng. 102 (1980) 263, https://doi.org/10.1115/1.3266190.
[33] N.H. Tay, M. Belusko, F. Bruno, An effectiveness-NTU technique for characterising tube-in-tank phase change thermal energy storage systems, Applied Energy 91 (2012) 309–319.
[34] K.A.R. Ismail, M.M. Gongalves, Effectiveness NTU performance of finned PCM storage unit, WIT Transactions on Modelling and Simulation 6 (1993), https://doi.org/10.2495/MB930291.
[35] A. Lázaro, M. Delgado, A. König-Haagen, S. Höhlein, G. Diarce, Technical performance assessment of phase change material components, in: SHC 2019 International Conference on Solar Heating and Cooling for Building and Industry, Santiago de Chile, Chile, 4–7 November 2019, 2019.
[36] S. Pinnau, Strömungs- und kältetechnische Optimierung von Latentkältespeichern, Abschlussbericht, Dresden, 2009.
[37] Brüggemann, D.; König-Haagen, A.; Kasibhatla, R.R.; Höhlein, S.; Glatzel, U.; Völkl, R.; Agarkov, N. *Entwicklung makroverkapselter Latentwärmespeicher für den Transport von Abwärme (MALATrans)*. Abschlussbericht: Laufzeit: 01.07.2013 bis 31.12.2016, Bayreuth, 2017.
[38] A. Hauer, W. van Helden, A. Abdi, T. Aigenbauer, M. Angerer, M. Bahrami, L. Baldini, D. Bauer, R. Bayón, N. Beaupéré, et al., IEA SHC Task 58/Annex 33: Material and Component Development for Thermal Energy Storage, 2020.
[39] G. Wang, C. Xu, W. Kong, G. Englmair, J. Fan, G. Wei, S. Furbo, Review on sodium acetate trihydrate in flexible thermal energy storages: properties, challenges and applications, Journal of Energy Storage 40 (2021) 102,780, https://doi.org/10.1016/j.est.2021.102780.
[40] G. Englmair, Y. Jiang, M. Dannemand, C. Moser, H. Schranzhofer, S. Furbo, J. Fan, Crystallization by local cooling of supercooled sodium acetate trihydrate composites for long-term heat storage, Energy and Buildings 180 (2018) 159–171, https://doi.org/10.1016/j.enbuild.2018.09.035.
[41] G. Englmair, C. Moser, S. Furbo, M. Dannemand, J. Fan, Design and functionality of a segmented heat-storage prototype utilizing stable supercooling of sodium acetate trihydrate in a solar heating system, Applied Energy 221 (2018) 522–534, https://doi.org/10.1016/j.apenergy.2018.03.124.
[42] G. Englmair, W. Kong, J. Brinkø Berg, S. Furbo, J. Fan, Demonstration of a solar combi-system utilizing stable supercooling of sodium acetate trihydrate for heat storage, Applied Thermal Engineering 166 (2020) 114,647, https://doi.org/10.1016/j.applthermaleng.2019.114647.
[43] Patil, A. Experimental study of coil and shell phase change material heat exchanger. Master Thesis; Dalhousie University, Halifax, Canada, 2020.
[44] Herbinger, F.; Groulx, D. Experimental comparative analysis of finned-tube PCM heat-exchangers' performance: under review. *Applied Thermal Engineering*.
[45] G. Wang, M. Dannemand, C. Xu, G. Englmair, S. Furbo, J. Fan, Thermal characteristics of a long-term heat storage unit with sodium acetate trihydrate, Applied Thermal Engineering 187 (2021) 116,563, https://doi.org/10.1016/j.applthermaleng.2021.116563.
[46] G. Wang, C. Xu, G. Englmair, W. Kong, J. Fan, S. Furbo, G. Wei, Experimental and numerical study of a latent heat storage using sodium acetate trihydrate for short and long term applications, Journal of Energy Storage 103 (2021) 588, https://doi.org/10.1016/j.est.2021.103588.
[47] G. Englmair, S. Furbo, M. Dannemand, J. Fan, Experimental investigation of a tank-in-tank heat storage unit utilizing stable supercooling of sodium acetate trihydrate, Applied Thermal Engineering 167 (2020) 114,709, https://doi.org/10.1016/j.applthermaleng.2019.114709.
[48] H. Mehling, L.F. Cabeza, *Heat and Cold Storage With PCM: An Up To Date Introduction Into Basics and Applications*, Springer-Verlag, Berlin, Heidelberg, 2008. ISBN 978-3-540-68,557-9.
[49] C. Rathgeber, S. Hiebler, E. Lävemann, P. Dolado, A. Lazaro, J. Gasia, A. de Gracia, L. Miró, L.F. Cabeza, A. König-Haagen, et al., IEA SHC Task 42/ECES Annex 29 – a simple tool for the economic evaluation of thermal energy storages, Energy Procedia 91 (2016) 197–206, https://doi.org/10.1016/j.egypro.2016.06.203.
[50] T. Xu, E.N. Humire, S. Trevisan, M. Ignatowicz, S. Sawalha, J.N. Chiu, Experimental and numerical investigation of a latent heat thermal energy storage unit with ellipsoidal macro-encapsulation, Energy 238 (2022) 121,828, https://doi.org/10.1016/j.energy.2021.121828.
[51] Burger, D.; Hagelstein, G.; Klünder, F.; Gschwander, S. *Innovative Prozesswärmespeicher mit organischen Latentmaterialien - Prolatent*. Abschlussbericht, Freiburg.
[52] C. Rathgeber, M. Helm, S. Hiebler, Energiespeicher für die Energiewende: Salzhydratbasierte Niedertemperatur-Latentwärmespeicher, Chemie Ingenieur Technik 90 (2018) 193–200, https://doi.org/10.1002/cite.201700049.
[53] M. Helm, K. Hagel, W. Pfeffer, S. Hiebler, S. Schweigler, D. Anders, Komponenten- und Systementwicklung: Solares Heizen und Kühlen mit Absorptionskältemaschine

und Latentwärmespeicher, Abschlussbericht; Laufzeit des Vorhabens: 01.10.2009 bis 30.09.2012, Verlängerung bis 30.09.2013, Garching, 2013.